

The Effects of Wind Farm Wakes on Freezing Sea Spray in the Mid-Atlantic Offshore Wind Energy Areas

David Rosencrans^{1,2}, Julie K. Lundquist^{1,2,3}, Mike Optis^{2,4}, and Nicola Bodini²

¹Department of Atmospheric and Oceanic Sciences, University of Colorado, Boulder, 80303, USA

²National Renewable Energy Laboratory, Golden, 80401, USA

³Renewable and Sustainable Energy Institute, Boulder, 80303, USA

⁴Veer Renewables, Courtenay, V9N 9B4, Canada

Correspondence to: David Rosencrans (David.Rosencrans@Colorado.edu)

Abstract

The U.S. is expanding its wind energy fleet offshore where winds tend to be strong and consistent. In the mid-Atlantic, strong winds, which promote convective heat transfer and wind-generated sea spray, paired with cold temperatures can cause ice on equipment when plentiful moisture is available. Near-surface icing is induced by a moisture flux from sea spray, which poses a risk to vessels and crews. Ice accretion aloft on turbine rotors and blades occurs when from liquid precipitation and in-cloud icing at temperatures below freezing. Ice accretion induces present and can load and fatigue on mechanical parts which reduces turbine-blade performance and power production and introduce extra load and fatigue on the turbine. Thus, it is crucial to understand the icing hazard across the mid-Atlantic. We analyze Weather Research and Forecasting model numerical weather prediction simulations at coarse temporal resolution over a 210-year period to assess freezing events over the long-term record and at finer granularity over the 2019–2020 winter season to identify the post-construction turbine impacts. Over the 2019–2020 winter season, results suggest that sea-spray-induced icing can occur up to 676 hours per month at 10 m at higher latitudes. Freezing-Icing events during this season typically occur during cold air outbreaks (CAO), which are the introduction of cold continental air over the warmer maritime surface. During the 2019-2020 winter season, cold air outbreaks CAO and lasted a total duration of 253-202 hours. While not all FSS events occurred during CAO over the 21 year period, all CAO events had FSS present. Over the 20-year period, all cold air outbreak events coincide with freezing conditions, although not all freezing events are cold enough to signify a cold air outbreak. Further, we assess the turbine-atmosphere impacts of wind plant installation on icing using the fine-scale simulation data set. Wakes from large wind plants reduce the wind speed, which mitigates the chance for freezing tearing initiation of sea spray off white-capped waves. Conversely, the near-surface turbine-induced introduction of cold air in frequent wintertime unstable conditions enhances the risk for freezing. Overall, the turbine-atmosphere interaction causes a net-small mitigation-reduction of freezing-FSS hours within the wind plant areas, with a reduction up to 157 hours in January at the 10 and 20 m heights at 20 m in January 2020.

1 Introduction

The offshore wind energy industry is undergoing rapid growth to supply emissions-free energy to the electrical grid. Across the mid-Atlantic outer continental shelf (OCS), the installed capacity could reach 30 GW by 2030

38 ~~{Citation}(White House, 2021).In the U.S., offshore capacity targets are approaching 40 GW by 2040 (Musial et al.,~~
39 ~~2022)(Musial et al., 2022).~~ Capacity expansion into relatively cold offshore regions will subject turbines to harsher
40 wintertime conditions, which necessitate an understanding of the hazards that marine icing poses to offshore wind
41 turbines, service vessels, and crew safety.

42
43 Ice accretion reduces the aerodynamic efficiency of the turbine blade, which hinders energy capture and annual
44 energy production (Battisti et al., 2006; Kraj and Bibeau, 2010; Wei et al., 2020). Ice can remain on the rotors even
45 after freezing conditions end, as slow natural processes such as ice shedding and melting extend the limitation to
46 energy yield (Gao and Hong, 2021). ~~One study found that excessive icing induced a power loss of 63 % for a single~~
47 ~~turbine over a 51-h icing event~~~~Some observations indicate that excessive icing can reduce torque enough that blade~~
48 ~~rotation stops entirely, causing up to 80 % reduced power production for a single turbine. (Gao and Hu, 2021).~~
49 ~~Investigating a 2050 future capacity expansion scenario, Novacheck et al. (2021) found that onshore icing events~~
50 ~~could reduce wind energy generation by 7 % and 10 % over two case study events using 65 % variable renewable~~
51 ~~energy penetration. For this scenario, Minnesota and Wisconsin would experience 75 % reduced wind energy~~
52 ~~generation during a daylong case study period, causing reliance on ramped up local gas generation and interregional~~
53 ~~transmission to meet the load.~~~~Faster winds in cold air outbreaks (CAO)during cold front passages can enhance~~
54 ~~wind-energy supply during high-load cold-weather events, although, following frontal passages, the combination of~~
55 ~~cold temperatures and slow wind speeds following frontal passage may pose severe challenges for utility grid~~
56 ~~planners (Novacheck et al., 2021). Despite the energy losses from ice accretion, various strategies can mitigate or~~
57 ~~even prevent ice accretion altogether (IEA, 2018; Madi et al., 2019).~~ While turbine blade icing is well studied (IEA,
58 2018; Martini et al., 2021; Contreras Montoya et al., 2022), icing near the turbine base, ~~affecting operations and~~
59 ~~maintenance activities,~~ is not. ~~Some turbines have icing detection and mitigation technology included at added cost,~~
60 ~~although current strategies need improvement (Madi et al., 2019).~~

61
62 The leading causes for low-level offshore icing are wave-impact and wind-induced sea spray (Dehghani-Sanij
63 et al., 2017). Sea spray provides nuclei for ice clouds at high latitudes where airborne dust is sparse, being lofted by
64 bursting bubbles and droplets from white-capped waves (Russell, 2015; Dehghani-Sanij et al., 2017). Ice
65 accumulation from spray raises the center of gravity of ships, which can cause loss of stability and lead to capsizing
66 (Guest and Luke, 2005). ~~Observations suggest that the liquid droplets torn off of white caps, referred to as spume,~~
67 ~~experience a marked increase in concentration with strong winds above 9 m s⁻¹ (Ross and Cardone, 1974; Monahan~~
68 ~~et al., 1983; Monahan and MacNiocail, 1986). Further, spray particles more easily supercool with cold sea surface~~
69 ~~temperatures (SST) below 7° C and at air temperatures below the freezing point for saline ocean water at -1.7° C~~
70 ~~(U.S. Navy, 1988; Guest and Luke, 2005).~~ Ice accumulation is believed to have caused the recent losses of three
71 ships, including 1) the *Destination*, which sank near St. George Island, Alaska in 2017- ~~(Kraegel, 2018)(Destination~~
72 ~~likely sank after accumulating ice in heavy freezing spray, report says, 2023);~~ 2) the *Scandies Rose*, which sank
73 southeast of Kodiak, Alaska, in 2019- ~~(NTSB, 2021)(NTSB announces the probable cause of the sunken Seandies~~
74 ~~Rose, 2023);~~ and 3) the *Onega*, which sank in the Barents Sea in 2020 ~~(being believed to cause sinking of fishing~~

Formatted: Font: (Default) Times New Roman, 10 pt,
Font color: Auto

Formatted: Font: (Default) Times New Roman, 10 pt,
Font color: Auto

Formatted: Not Superscript/ Subscript

75 ~~boat in Barents Sea, 17 missing, 2023)(Nilsen, 2020)~~. To mitigate ice-induced accidents, inclement weather
76 forecasts are furnished for coastal waters. A Coastal Waters Forecast, delivered by the National Weather Service,
77 will contain a “freezing spray advisory” if freezing water droplets can accumulate on vessels due to a combination
78 of ~~sea surface temperature (SST)~~SST, wind speed, air temperature, and vessel motion (Glossary - NOAA’s National
79 Weather Service, 2023). At accumulation rates greater than 2 cm h⁻¹, the advisory becomes a “heavy freezing spray
80 watch”.

81
82 Wind turbines can modify the amount and severity of freezing-icing conditions via competing effects. Enhanced
83 turbulence caused by spinning blades transports ~~temperatures-heat(either warmer or colder)~~ from aloft to lower
84 altitudes within the rotor-swept region or near the surface. In stable stratification, warmer potential temperatures are
85 transported downward, which introduces a near-surface warming effect, and vice versa in unstable conditions (Fitch
86 et al., 2013; Rajewski et al., 2013; Xia et al., 2016; Siedersleben et al., 2018; Tomaszewski and Lundquist, 2020).
87 However, recent research suggests taller turbines may reverse this phenomenon (Golbazi et al., 2022) depending on
88 the depth of the atmospheric boundary layer (Quint et al., 2024). ~~(Quint et al., 2024)~~. As the winter months feature
89 more frequent unstable stratification along the U.S. East Coast (Bodini et al., 2019), turbine-induced cooling may
90 increase the potential for near-surface icing/freezing. In contrast, turbines harness momentum from the flow, which
91 reduces the downwind wind speed (Nygaard, 2014; Platis et al., 2018; Schneemann et al., 2020). A reduction in
92 wind speed conversely reduces the potential for icing (Dehghani-Sanij et al., 2017). Thus, it is crucial to understand
93 how large-scale wind deployment across the mid-Atlantic will modify the regularity and intensity of freezing sea
94 spray (FSS) conditions.

95
96 Herein, we employ numerical weather prediction modeling to quantify the baseline offshore icing risk and the
97 wind plant post-~~production-construction~~ effects. Section 2 outlines the modeling setup and discusses the techniques
98 for discerning freezing-icing conditions events and cold air outbreak events. Section 3 reports results for the
99 spatiotemporal icing risk, causal factors, and the adjustments by wind plants. Section 4 offers concluding remarks
100 and discussion.

102 2 Methods

103 2.1 NOW-23

104 We explore annual variability of freezing-FSS conditions using the 2023 National Offshore Wind (NOW-23)
105 data set (NREL, 2020; Bodini et al., 2024). This data set provides-quantifies an offshore wind resources -spanning
106 all offshore regions of the United States at 5-min resolution for up to 22 more than 20 years using the Weather
107 Research and Forecasting (WRF) model version 4.2.1 (Powers et al., 2017). ~~For the mid-Atlantic region, NOW-23~~
108 ~~was validated against observations from three ZephIR ZX300M floating lidars (Pronk et al., 2022)~~. We acquire -
109 model output at an hourly temporal resolution for the 210-year period from 01 January 2000 to 31 December 2020.
110 ~~NOW-23 employs the Weather Research and Forecasting (WRF) model (Powers et al., 2017) version 4.2.1.~~ A parent
111 domain feeds into an inner nested domain with horizontal grid resolutions of 6 km and 2 km, respectively. Both
112 domains have-incorporate a vertical grid resolution of 5 m near the surface with stretching to 45 m aloft, using 61

Commented [JL1]: Daphne’s micrometeorological impacts paper is up online now so you can cite that.

113 vertical levels up to a 50 hPa top. The European Centre for Medium Range Weather Forecasts 5 Reanalysis (ERA5)
114 dataset supplies hourly initial and boundary conditions at a 30 km resolution to WRF (Hersbach et al., 2020). NOW-
115 23 employs the MYNN2 planetary boundary layer and surface layer (Nakanishi and Niino, 2006) schemes, eta
116 microphysics (Ferrier et al., 2002), the Noah Land Surface Model (Tewari et al., 2004), the rapid radiative transfer
117 model for shortwave and longwave radiation (Iacono et al., 2008), and the Kain–Fritsch cumulus parameterization
118 (Kain, 2004) in the outmost domain only. [For the mid-Atlantic region, NOW-23 was validated against observations](#)
119 [from three ZephIR ZX300M floating lidars \(Pronk et al., 2022\).](#)

120 2.2 NOW-WAKES

122 We explore the seasonal variability and impacts of wind plants on icing conditions using high-fidelity numerical
123 weather prediction simulations over the period 01 September 2019 to 31 August 2020. These validated WRF version
124 4.2.1 simulations are described in detail in ~~(Rosencrans et al., (2024) Rosencrans et al. (2023))~~ but are summarized
125 here for the reader’s convenience. This period is chosen for the availability of lidar measurements for validation of
126 the wind speed profile. A parent domain hosts an inner nest with horizontal grid resolutions of 6 km and 2 km,
127 respectively ([Figure 1](#)). Both domains ~~have incorporate~~[include](#) a vertical grid resolution of 10 m near the surface
128 with stretching aloft, using 54 vertical levels up to a 50 hPa top. The inner domain outputs data at an instantaneous
129 history file frequency of 10 minutes. Constant time steps are set to 18 s and 6 s in the outer and inner domains,
130 respectively. Initial and boundary conditions are also supplied by the hourly 30 km ERA5 dataset (Hersbach et al.,
131 2020). Lower boundary conditions are provided as SST by the UK Met Office Operational Sea Surface Temperature
132 and Sea Ice Analysis dataset (Donlon et al., 2012) and show good agreement during validation against mid-Atlantic
133 bight buoys (Redfern et al., 2023). Physics parameterizations include the MYNN2 planetary boundary layer and
134 surface layer (Nakanishi and Niino, 2006), the Noah Land Surface Model (Niu et al., 2011), the New Thompson
135 microphysics (Thompson et al., 2008), the rapid radiative transfer model for longwave and shortwave radiative
136 transfer (Iacono et al., 2008), and the Kain–Fritsch Cumulus (Kain, 2004) schemes. The Kain–Fritsch cumulus
137 parameterization applies to the parent domain only. [We incorporate spectral nudging to relax model output toward](#)
138 [the ERA5 boundary conditions in the inner domain. We apply a cutoff wavenumber of 3](#) (Gómez and Miguez-
139 Macho, 2017), [above which model dynamics may resolve freely. No nudging is applied beneath the boundary layer](#)
140 [height.](#)

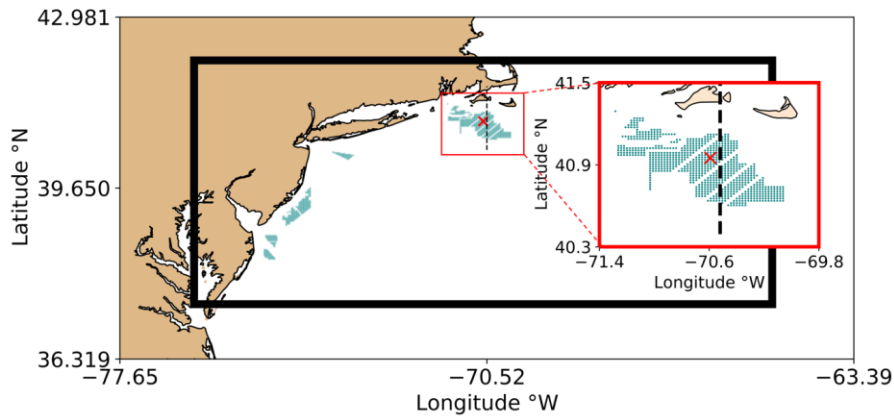


Figure 1. Modeling domains. The entirety of the outer domain with inner domain is shown, outlined by the black rectangle. The red square is zoomed in on the Rhode Island–Massachusetts (RIMA) block to enhance visibility. Turbines are shown as teal dots. The red “X” indicates the point of interest (POI) where time series are acquired. The dashed black line is a cross section extending through the RIMA block.

We incorporate the effects of wind turbines using the WRF wind farm parameterization (WFP) (Fitch et al., 2012). WFP simulations feature wind plant layouts of the lease areas and include 1,418 turbines (Figure 1, Table 1). The WFP incorporates the effects of turbines by implementing a drag-induced deceleration of wind flow and an addition of turbulence at model levels intersecting the rotor area. We execute WFP simulations adding both 0 % and 100 % turbulent kinetic energy (TKE) (Rosencrans et al., 2024) (Rosencrans et al., 2023), although a smaller value of 25 % in some cases agrees better with neutrally stratified large-eddy simulations (Archer et al., 2020). The differences in icing results, the number of icing hours between 0 % and 100 % added TKE are slight, so we report those from 100 % added TKE only. Thus, for the remainder of this article we refer to the 100 % added TKE simulation as “WFP”. This work utilizes 12 MW GE Haliade wind turbines with a 138 m hub height and 215 m rotor diameter, which is scaled by Beiter et al. (2020) from a 15 MW reference turbine. We carry out separate simulations using both no wind farms (NWF) and wind farms (WFP) for the full year-long period from 01 September 2019 to 31 August 2020 (Table 1).

Table 1. List of NOW-WAKES WRF simulations characterized by turbine characteristics. The simulation period spans 01 September 2019 to 01 September 2020.

Simulation Type	Acronym	Turbine rated power Type	Added TKE	# Turbines
No Wind Farms (NWF)	NWF	N/A	N/A	0
Wind Farm Param. (WFP)		12 MW	0%	1,418

Formatted: Check spelling and grammar

Formatted: Check spelling and grammar

Formatted: Check spelling and grammar

Formatted Table

Wind Farm Parameterization-(WFP)	WFP	12 MW	100 %	1,418
-------------------------------------	-----	-------	-------	-------

163

164 **2.3 Freezing Icing hours detection**

165

165 Ice accretion occurs when supercooled water freezes upon contact with objects. The largest contributions to sea
 166 spray icing are provided by the bursting of bubbles and advection of spray from white-capped waves (Dehghani-
 167 Sanij et al., 2017). ~~Further aloft, supercooled water can be introduced by liquid precipitation and fog.~~ In the presence
 168 of moisture, ~~there are~~ three key variables ~~that~~ dictate offshore freezing conditions: wind speed, SST, and air
 169 temperature (Overland et al., 1986; Overland, 1990; Guest and Luke, 2005; Dehghani-Sanij et al., 2017; Line et al.,
 170 2022).

171

172 We ~~define detect input freezing FSS~~ conditions following ~~the most liberal~~ common thresholds defined by the
 173 latter studies ~~(Guest and Luke, 2005; Dehghani-Sanij et al., 2017; Line et al., 2022)~~, ~~which produce more freezing~~
 174 ~~events, to compensate for a negative wind speed bias in unstable stratification (Rosencrans et al., 2023), which~~
 175 ~~mitigates freezing occurrence.~~ These criteria require 1) wind speeds in excess of 9 m s⁻¹, 2) air temperatures below
 176 -1.7° C, and 3) SST less than 7° C. ~~Air temperature and SST thresholds can range between -2° C and -1.7° C and~~
 177 ~~between 5° C to 8.9° C, respectively, as reviewed by (Dehghani-Sanij et al., (2017). As such, we provide a~~
 178 ~~sensitivity assessment for the full range (Appendix B). The surface~~ skin temperature (WRF output variable “TSK”)
 179 is ~~used assessed~~ because the SST field inherits coarse blocks of missing data around coastlines from the ERA5
 180 dataset. The resulting spatial maps are masked by the land use (WRF output variable “LU_INDEX”) to ensure
 181 ~~freezing that icing~~ conditions over land are not counted. The number of 10 min timestamps where these criteria are
 182 met each month are recorded for all simulations. ~~exp~~

183

184 ~~Sea spray induced icing can affect structural integrity, blade aerodynamics, and crew safety.~~ As sea spray often lofts
 185 to between 5 and 20 m above sea level (Dehghani-Sanij et al., 2017), we ~~detect also quantify sea spray-induced~~
 186 ~~icing possible icing conditions~~ at the ~~lowest model level of 10 m~~ and at 20-m heights. For the 20 m conditions, we
 187 ~~use 20 m air temperatures but use 10 m wind speeds~~ as those winds are responsible have been ~~for linked to the~~
 188 ~~continue to detect fast wind speeds at the 10 m height for~~ generation of spray off white-capped waves (Dehghani-
 189 Sanij et al., 2017; Guest and Luke, 2005; Line et al., 2022; Ross and Cardone, 1974; Monahan et al., 1983; Monahan
 190 and MacNiocaill, 1986).

191

192 ~~We~~ Due to the height constraint of sea spray particles, we ~~further consider both precipitation-based and in-cloud~~
 193 ~~icing riming conditions~~ at the 138 m hub height by ~~including assessing an additional different eritericriteria for on for~~
 194 ~~the 1) the nonzero~~ presence of liquid rain water (WRF variable “QRAIN”) that may become supercooled at
 195 temperatures less than 0° C, 2) ice (WRF variable “QICE”), and 3) the aggregation from snow (WRF variable
 196 “QSNOW”) (Parent and Ilina, 2011; ISO, 2017), ~~as precipitation induced ice can generate a considerably higher~~
 197 ~~ice accretion rate than fog induced icing (Gao and Hong, 2024). Further, we detect cloud or fog formation when 4)~~
 198 ~~the relative humidity (RH) is greater than or equal to 100% following: (Parent and Ilina, 2011)~~

Formatted: Indent: First line: 0", Line spacing: single

Commented [JL2]: I think this sentence belongs somewhere else, in the introduction perhaps?

199

$$e_s = e_0 \exp \left[\frac{b(T - T_1)}{(T - T_2)} \right] \tag{1}$$

200

$$w_s = \frac{\epsilon e_s}{p - e_s} \tag{2}$$

201

$$RH = \frac{w}{w_s} \times 100\% \tag{3}$$

202

203

204

205

206

207

208

209

210

211

212

213

214

215

216

217

218

219

220

221

222

223

224

225

226

227

228

229

2.4 Ice accumulation rate

A predictability function assesses the likelihood for freezing in the presence of sea spray. We assess the predictability of icing conditions at the point of interest (POI) in the Rhode Island/Massachusetts (RIMA) block (Figure 1) separately from the NOW-WAKES and the NOW-23 datasets. The predictability (PPR) for sea spray-induced ice formation follows:

$$PPR = \frac{V_a(T_f - T_a)}{1 + 0.4(T_s - T_f)} \tag{4}$$

where V_a is the wind speed, T_f is the temperature threshold of -1.7°C , T_a is the air temperature, and T_s is the SST (Guest and Luke, 2005; Overland et al., 1986; Overland, 1990). A humidity variable is not present in Eq. (4) due to the assumption that sea spray introduces a constant source of moisture during fast winds, that of which is required for nonzero PPR. A group of successive timestamps with nonzero PPR are considered the same event. Separate flagged timestamps occurring within 24 hours of each other span the same synoptic regime (Winters et al., 2019), and so the entire duration between the two flagged timestamps is considered one event. We additionally tested a threshold of 72 hours to account for synoptic conditions spanning a longer duration but found that one FSS event lasted for over a week and our three FSS criteria were only met 8 % of the time during the event. As such, the 72-h threshold was not justified.

Table 2. Icing rate by PPR. Rows delineate the icing predictability (PPR value), icing class, and ice accretion rate. Columns delineate the icing rate per PPR range. From Guest and Luke (2005).

PPR	<0	0–22.4	22.4–53.3	53.3–83.0	>83.0
Icing Class	None	Light	Moderate	Heavy	Extreme
Icing Rate [cm h ⁻¹]	0	<0.7	0.7–2.0	2.0–4.0	>4.0

The magnitude of PPR can determine the rate of ice accretion (Table 2). The ice accretion rates are a general guideline developed for 20 to 75 m long vessels; specific rates depend on the type of ship, its load, heading relative

Formatted: Font:

Formatted: Font:

Formatted: Font: Times New Roman, Not Italic

Formatted: Indent: First line: 0"

Formatted: Font:

Formatted: List Paragraph, Bulleted + Level: 1 + Aligned at: 0.5" + Indent at: 0.75"

Formatted: Indent: First line: 0.25"

230 to the prevailing wind direction, and its handling characteristics (U.S. Navy, 1988; Guest and Luke, 2005). For
231 instance, a larger ship requires faster winds and taller waves for sea-spray-induced ice to accumulate on a higher
232 deck but is more vulnerable to the prevailing wind direction due to reduced maneuverability. It is not known how
233 these icing rates would apply to wind turbines or to the vehicles used to access offshore wind turbines.

236 2.5 Cold air outbreak detection

237 Freezing conditions can be stimulated by the advection of cold continental air over a warmer maritime surface.
238 The resulting temperature profile induces-causes thermal instability, which causes-can induce filamentary convective
239 rolls that align to make cloud “streets” with parallel columns of ascending and descending air that transform into
240 open convective cells further offshore (Geerts et al., 2022). Convective rolls can be used to identify cold air outbreak
241 (CAO) (Atkinson and Wu Zhang, 1996; Geerts et al., 2022) and may also contribute moisture for in-cloud icing if
242 the lifting condensation level is at or below rotor-swept heights. A quantitative approach proposed by Vavrus et al.
243 (2006) identifies a cold air outbreak (CAO) by the magnitude and duration of anomalous air temperature, which we
244 apply at the POI (Figure 1). This strategy requires that the near-surface temperature be at least 2 standard deviations
245 below the wintertime average following Eq. (52):

$$246 T < \bar{T} - 2(\sigma) \quad (52)$$

247 where T is the 240 m temperature, \bar{T} is the average 10 m temperature during-over the entire wintertime period, and σ
248 is the standard deviation. The wintertime period spans November through March at a 10 min frequency to account
249 for all non-zero-freezing predictability events. Again, successive timestamps with detected CAO are considered a
250 single event, and separate events occurring within a 24 h span are conglomerated into the same event.

252 2.6 Atmospheric stability

253 Turbulence from wind turbines modifies the near-surface temperature based on the atmospheric stability or
254 stratification. We calculate the modeled atmospheric stability using the Obukhov Length (L) (Monin and Obukhov,
255 1954) (Eq. 63), which delineates the height above the surface at which buoyant turbulence equals mechanical shear
256 production of turbulence, at a point centered on the RIMA block of lease areas:

$$257 L = -\frac{u_*^3 \bar{\theta}_v}{\kappa g (\overline{w' \theta_v'})} \quad (63)$$

258 where u_* (UST in WRF output) is the friction velocity, θ_v is the virtual potential temperature, κ is the von Kármán
259 constant of 0.4, g is gravitational acceleration of 9.81 m s^{-1} , and $\overline{w' \theta_v'}$ (HFX in WRF output) is the surface dynamic
260 heat flux converted into kinematic heat flux. Negative lengths between 0 m and -500 m imply unstable stratification
261 due to a positive heat flux (Gryning et al., 2007; Archer et al., 2016). Conversely, lengths between 0 m and 500 m
262 imply stable stratification due to a negative heat flux. Lengths approaching negative or positive infinity imply
263 neutral stratification, as buoyancy is no longer a dominating factor. Each 10 min timestamp from the NWF run is
264 assigned a stability classification from November 2019 to March 2020.

266 **3 Results**

267 **3.1 Spatial variability of freezing-icing conditions**

268 The ~~percentage-of-occurrence~~~~prevalence-of~~ freezing-icing conditions exhibits regional variability. The
269 commonality of freezing-icing increases toward higher latitudes and near the coast where cold continental air
270 advects over the ocean during the winter (Figure 2). In general, the spatial icing pattern during the 2019–2020 winter
271 season (Figure 2a) matches well with the pattern over the 210-year period (Figure 2b) although the 2019–2020
272 season is relatively mild compared to other winters (Figure 2, Figure 3a). Freezing-Icing conditions shadow the mid-
273 Atlantic coast but occur less often along the New Jersey Bight where wind speeds decrease and air and sea
274 temperatures warm. The commonality-prevalence of freezing conditions extends furthest offshore southeast of
275 Nantucket and enhances in the Long Island Sound; both regions feature local minima in mean January 2020 SST
276 less than 5° C. The Long Island Sound is flanked by land to the north and south which amplifies the presence of cold
277 air. In addition, mean wind speeds maximize to the east of Cape Cod and Nantucket (Bodini et al., 2024) which
278 increases the number of hours that wind-generated spray is present. Finally, t (Bodini et al., 2023) To the north, the
279 cyclonic current in the Gulf of Maine transports cold-surface water southward. East of Cape Cod, this current
280 bifurcates around the Georges Bank, and a branch feeds cold fresh water into the mid-Atlantic (Chapman et al.,
281 1986). The number of icing hours may be further exacerbated when pPredominant northerly winter winds instigate
282 onshore Ekman transport towards the coast, which is favorable for downwelling (Shcherbina and Gawarkiewicz,
283 2008b). However, downwelling is not always supported, as the mixed layer stratification is dominated by salinity
284 (Shcherbina and Gawarkiewicz, 2008a), leaving a cold pool near the surface.

285

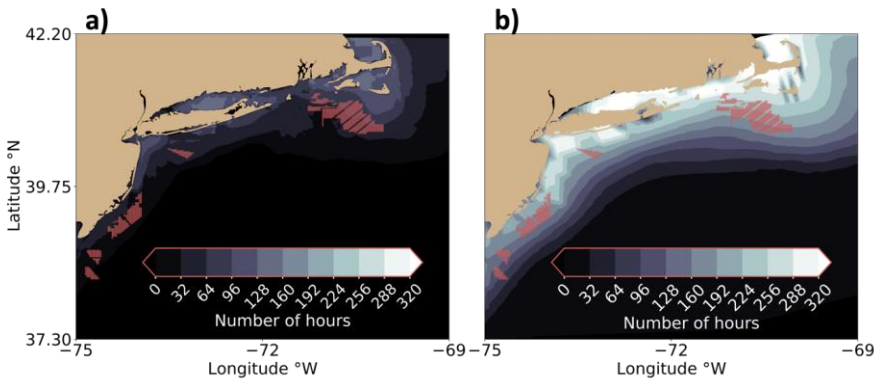
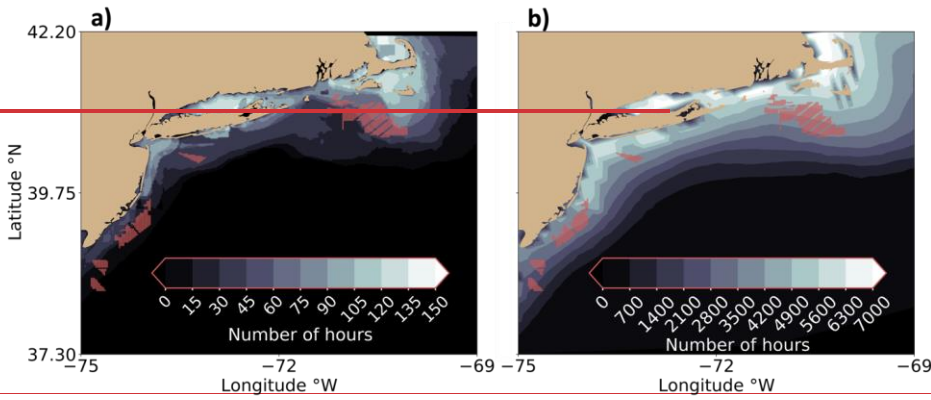


Figure 2. The number of hours freezing-FSS conditions occur at 10 m during (a) the November 2019 to March 2020 period inat 10-m-in-NWF and (b) the mean the November to March period from 2000 to 2020 in NOW-23. Lighter contouring indicates more freezing hours. Red dots represent turbine locations in-(a)but do not exist in (a) or (b) andandbut are shown for qualitative-comparisonreference. -

Freezing-Icing conditions exhibit seasonal variability in NWF, starting at 0 hours in November, increasing through the winter, and falling to 0 again by April at all heights (Figure 3 and Figure. A1–A3). At the 10 m altitude, freezing-FSS conditions occur most often in January, up to 676 hours, with an offshore spatial extent of 597,420-292 km², or roughly 12.3 times the area of the wind plants. At 20 m, freezing-FSS conditions also occur most often in January, up to 6870 hours, covering a total area of 61,7932-64 km², or roughly 12.83 times the area of the wind plants (Figure A2). The 20 m height experiences more freezing hours than the 10 m height because average wind speeds are at least 0.25 m s⁻¹ faster around Nantucket, Cape Cod, and the Long Island Sound. The 138 m hub height

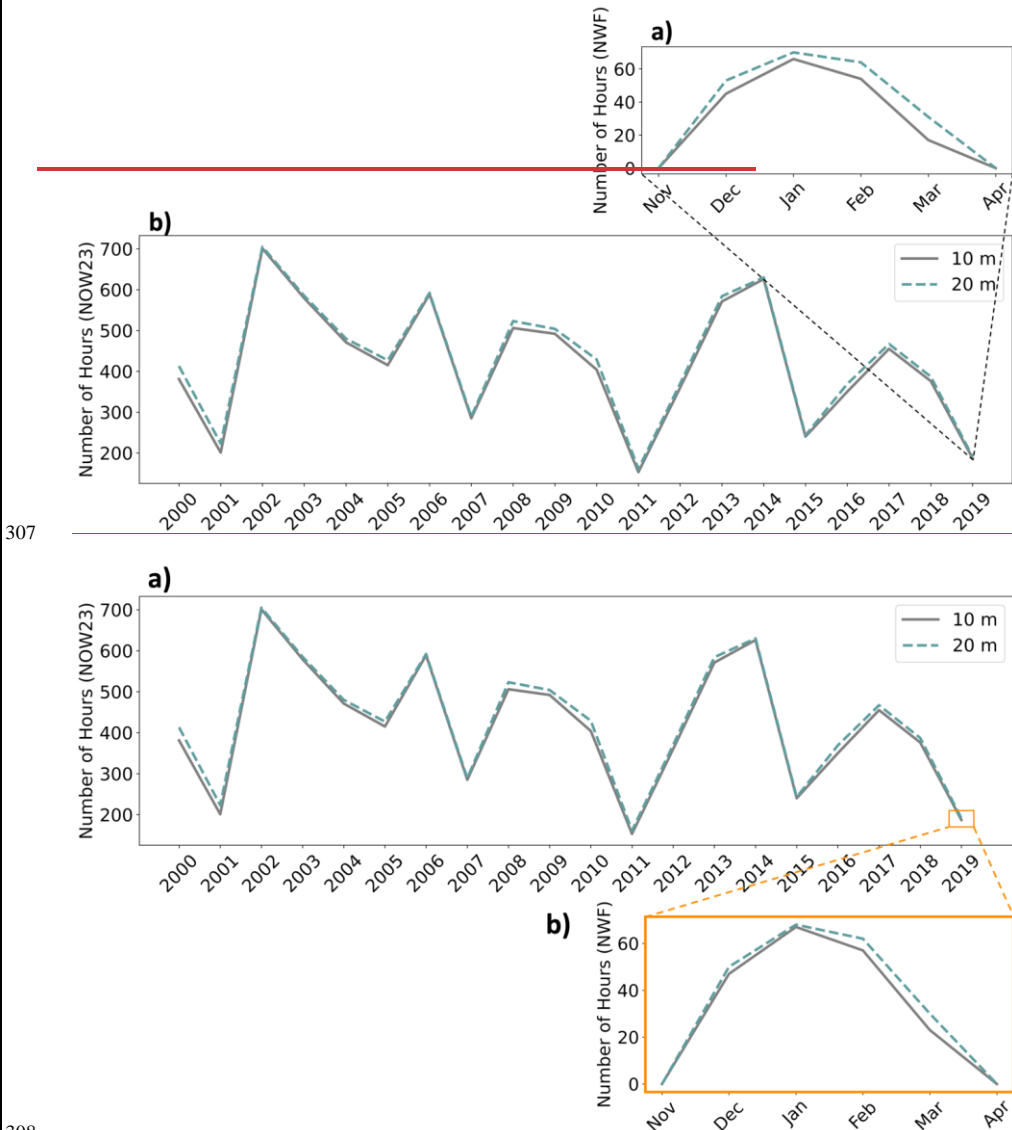
Formatted: Normal, Left, Indent: First line: 0", Line spacing: single

Commented [DR3]: Are temperatures also typically colder too?

Commented [DR4R3]: We don't assess wind speeds here anymore. Assess temperature only

302 ~~has aattains the smaller-largest~~ maximum of ~~29-119~~ hours during January in the Gulf of Maine, ~~with a band~~
303 ~~extending south from and to the east~~ Cape Cod, ~~posing no threat to the lease areas~~ (Figure A3), ~~with an offshore~~
304 ~~spatial extent of 291,012 km², or 60.2 times the area of the wind plants. Although wind speeds increase aloft, the~~
305 ~~regularity of liquid water is not as consistent, as is near surface sea spray.~~

306



307

308

309

310

311

Figure 3. The maximum number of freezing FSS hours over the OCS (a) seasonally-annually and (b) annually-seasonally from 2019 to 2020 in NOW-23. The zoomed orange cutout shows the seasonal variation over the 2019–2020 winter.

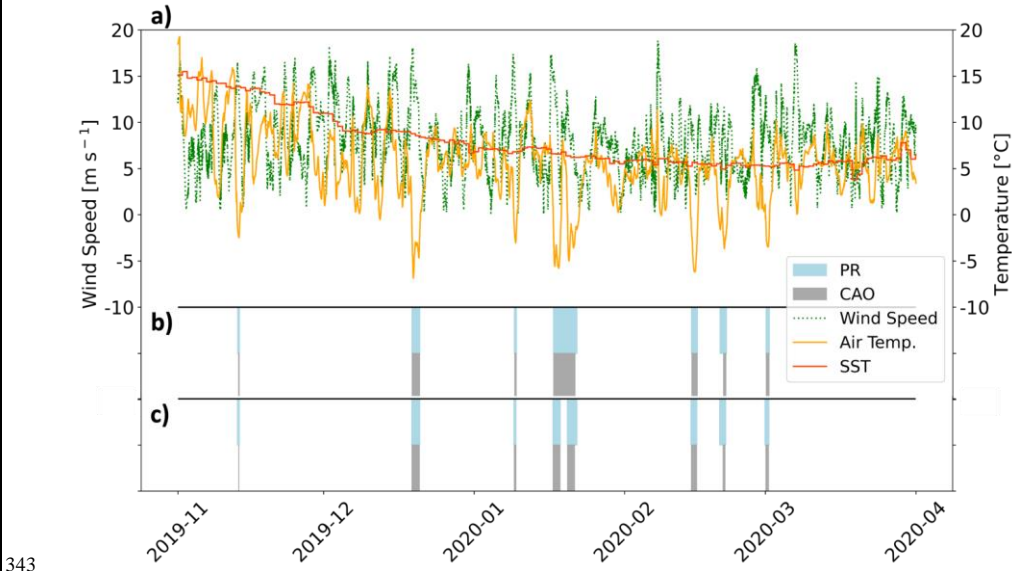
312 The 2019–2020 winter season was one of the mildest compared to other winters (Figure 3ab), as assessed using
313 the FSS detection criteria (Section 2.3). This winter season had the fewest few number of freezing icing hours
314 compared to other winters over the 210-year period, reaching 19482 hours in NWF or 187 hours in NOW-23 at 10
315 m. At 20 m, the 2019–2020 winter season contains 2108 hours in NWF or 191 hours in NOW-23. The greatest
316 number of freezing-icing hours occurs during the 2002–2003 season, with 701 total hours at 10 m and 705 hours at
317 20 m. While the 210-year slope shows a decrease, it is not statistically significant using the Mann–Kendall (M–K)
318 test (Hussain and Mahmud, 2019). P-values for the maximum number of icing hours (found across the OCS) (Figure
319 3ab) and for the number of freezing-hours at the POI (Figure 1) are 0.20 and 0.12, respectively. We additionally
320 applied the seasonal M–K test (Hirsch et al., 1982) to account for upward and downward trends throughout the year
321 on monthly mean PPR, monthly maximum PPR, and the monthly total number of icingfreezing hours at the POI.
322 Neither test returned a statistically significant trend.

323 **3.2 Freezing-Icing conditions and cold air outbreak**

324 Investigating all events with a non-zero freezing-PPR at the POI (Figure 1) reveals similar synoptic trends. We
325 identify seven events with freezing-sea-spray (FSS)FSS conditions with a total duration of 2533 hours from
326 November 2019 to March 2020. All times during the 2019–2020 winter period with nonzero PPR contain light ice
327 accumulation of less than 0.7 cm h^{-1} (Table 2). During each FSS event, higher relative pressure resided to the
328 southwest throughout the Great Plains, Appalachia, or the Great Lakes with lower relative pressure to the northeast
329 around Nova Scotia and Newfoundland. In the Northern Hemisphere, winds flow with higher pressure to the right
330 and lower pressure to the left (Wallace and Hobbs, 2006)(Ballot and Didericus, 1857). This flow regime results from
331 the balance between the pressure gradient force and the Coriolis force, which is a force introduced into the equations
332 of motion to account for acceleration on a non-inertial rotating reference frame (Ferrel, 1856). The largest pressure
333 gradient forces occurred during the two January events of upreaching to $4 \times 10^{-2} 4 \text{ hPa m}^{-1}$ per 100 km, or roughly 4
334 times the pressure gradient force required for a 10 m s^{-1} geostrophic wind in the midlatitudes (Parish et al., 2007).
335 Most events feature either an outflow boundary or a cold front in the mid-Atlantic. This pressure regime directs
336 quasi-geostrophic flow near the surface toward the southeast, introducing cold continental air offshore. During the
337 winter, the prevailing wind direction is northwesterly across the mid-Atlantic OCS (Bodini et al., 2019) because
338 regions of land mass feature higher surface pressure than the surrounding ocean and the Bermuda High retreats to
339 the east.
340
341



342



343

344 **Figure 4.** (a) Time series of wind speed (green dotted), 10 m air temperature (orange), and SST (red) from November
 345 2019 to April 2020 at the downwind edge of Vineyard Wind ([Figure 1](#)). Light-blue shading indicates the duration of
 346 nonzero PPR, and gray shading indicates the duration of detected CAO from (b) NWF and (c) NOW-23.

347
348 ~~Most All offshore freezing FSS events, assessed using PR, coincide with CAO. We detect ~~sevensix~~ CAO~~
349 ~~events in NWF with a total duration of ~~2020~~ hours (Figure 4b). The ~~typical-mean~~ durations of CAO events (~~29~~~~
350 ~~hours) are ~~seven3~~ hours shorter than FSS events (36 hours), with ~~78-980~~ % of flagged FSS timestamps having CAO~~
351 ~~present. Overall, six of the seven FSS events occur in conjunction with a CAO (b), with November air temperatures~~
352 ~~not cold enough to be flagged as CAO candidates. We note that in NWF, all seven FSS events coincide with CAO at~~
353 ~~the northeast edge of the RIMA block which is nearer to the introduction of cold continental air.~~

354
355 Common between events are fast wind speeds and cold 10 m air temperatures; SST plays a secondary role for
356 its weak temporal variability (Figure 4a). The average wind speed during FSS events is 10 m s⁻¹ with gusts
357 exceeding 15 m s⁻¹ during four events. Nonzero PPR does not occur until after the wind speed peaks, when cold air
358 temperatures sweep in, averaging minimum temperatures of -4.55° C (Figure 4a). This wind speed-temperature
359 dynamic can pose as challenges for grid planners because-if wind energy generation reduces during periods of high
360 demand for residential and commercial heating, especially in a future scenario with electrification of space heating of
361 peak heating load.

362
363 ~~Over~~During the 2019–2020 winter in the NOW-23 dataset, eight total events are flagged as candidates for FSS
364 because the longest event in January 2020 (Figure 4b) is split among two separate events; all eight events have a
365 corresponding CAO (Figure 4c). Over the 210-year period, all CAO events occur in conjunction with an FSS event
366 (positive PPR) (Fig. C1–Fig. C20). However, many FSS events occur without CAO present meaning that CAO is
367 only one of the drivers, and large interannual variability can exist. For instance, while 10097 % of CAO timestamps
368 concur with FSS during the 2011–2012 season, only 109 % do during the 2013–2014 season.

369
370 The 2019–2020 winter ice accumulation rate is similar to other winters. The average PPR during freezing
371 events from 2019 to 2020 is 4.3, which corresponds to a light ice accumulation rate of less than 0.7 cm h⁻¹ (Table 2).
372 Over the 210-year period, the average PPR among events is 8.1, which corresponds to the same accumulation rate.
373 The 2003–2004 winter period features the greatest mean PPR of 15.7, which also corresponds to a light ice
374 accumulation rate. During this periodwinter, a moderate risk for icing occurred 18 % of the time, and a heavy risk
375 occurred 3 % of the time, corresponding with icing rates between 0.7–2.0 cm h⁻¹ and 2.0–4.0 cm h⁻¹, respectively,
376 and possibly triggering heavy freezing spray watches in the NWS advisory.

377 Synoptic-scale teleconnection patterns can impact the likelihood of icing conditions. From December 2003 to
378 March 2004, the Pacific North Atlantic (PNA) cycle was positive. During the positive phase of PNA, a relative high-
379 pressure anomaly with anticyclonic wind flow exists over the western US that is conducive to northwesterly
380 transport of cold air over the East Coast (Vavrus et al., 2006). In addition, the entire November 2003 to March 2004
381 period featured a positive El Niño-Southern Oscillation (ENSO) index. Positive ENSO has been attributed to cooler
382 SSTs across the mid-Atlantic and northeasterly winds which advect cold air from the north (Alexander and Scott,

- Formatted: Font:
- Formatted: Font:
- Formatted: Font:
- Formatted: Font: (Default) Times New Roman, 10 pt
- Formatted: Font:
- Formatted: Font:

2002). Other teleconnection patterns, including the Arctic Oscillation and North-Atlantic Oscillation switched signs during this winter and are not discussed in greater detail.

Formatted: Font:

3.3 Modifications by wind plants

The near-surface cooling effect by rotor turbulence provides a subtle effect on freezing conditions is more probable in cold temperatures. In unstable conditions, which occur 64 % of the time from November 2019 through March 2020 in NWF assessed at the POI, wind turbines introduce near-surface cooling, which could increase the likelihood of icing. For instance, mean cooling and warming during unstable conditions reach magnitudes up to -0.041 K at the surface and 0.022 K within the rotor-swept region, respectively, along a cross section extending through the RIMA block (Figure 1, Figure 5b). During stable conditions, which occur 25 % of the time from November through March, cooling aloft reaches up to -0.34 K, and near-surface warming reaches 0.26 K (Figure 5a). Near-surface cooling exists adjacent to the wind plant cluster (Xia et al., 2016).

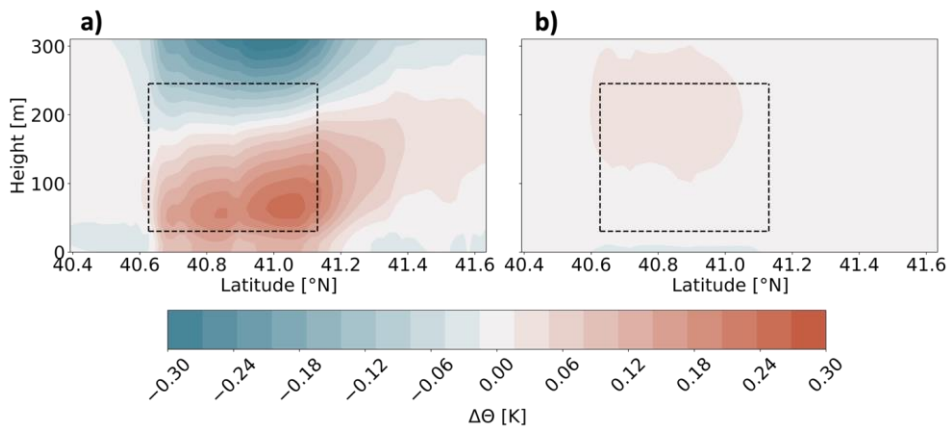
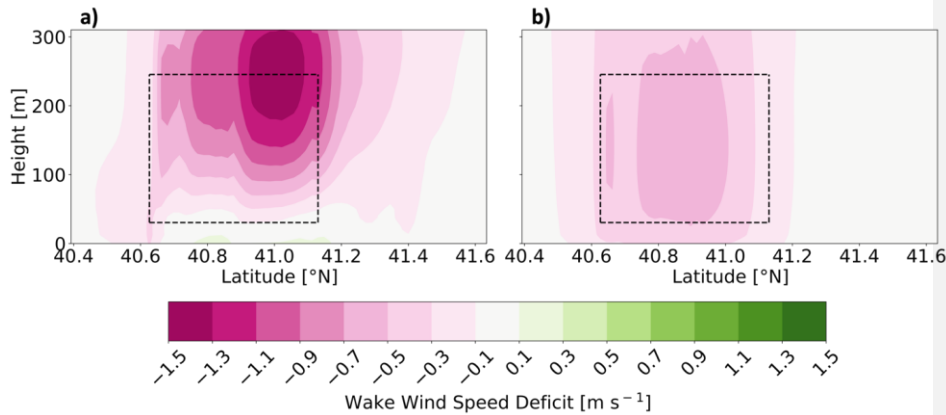


Figure 5. The mean (WFP-NWF) potential temperature difference during (a) stable stratification and (b) unstable stratification, from November 2019 to March 2020. The cross section spans the RIMA block of lease areas (Figure 1). Red contouring indicates warming, and blue indicates cooling. Dashed lines outline the wind plant area and rotor-swept region.

Conversely, the reduction of wind speeds in the wake modifies the chance for icing within the rotor-swept area and near the surface by reducing the production of white-capped waves and the wind-induced tearing of spray off waves. In stable conditions, the mean wake wind speed deficit is largest, reaching -1.4 m s^{-1} near the top of the rotor-swept plane, reducing the chance for freezing icing. Because vertical motion is suppressed in stable stratification, winds increase and flow around and under the wind plant area (Figure 6a), reaching a subtle enhancement near the surface of 0.187 m s^{-1} . In unstable stratification, available buoyant turbulence promotes mixing which transports momentum from above the rotor-swept region down to within the wake. The injection of

409 momentum allows wake wind speeds to recover, leaving a smaller maximum averaged wake deficit of -0.57 m s^{-1}
 410 (Figure 6b). There is no enhancement of wind speeds adjacent to the RIMA block along the cross section in unstable
 411 conditions.
 412



413
 414 **Figure 6. The mean (WFP-NWF) wind speed difference during (a) stable and (b) unstable stratification, from November**
 415 **2019 to March 2020. The cross section spans the RIMA block of lease areas (Figure 1). Pink contouring indicates a wind**
 416 **speed reduction, and green indicates wind speed enhancement. Dashed lines outline the wind plant area and rotor-swept**
 417 **region. Note the very small enhancement of wind speeds near the surface in stable conditions.**

418
 419 Despite near-surface cooling, net freezing-FSS conditions in WFP occur less often than in NWF when
 420 diagnosed using wind speed, air temperature, and SST criteria because of the wake wind speed reduction. At 10 m,
 421 the turbine–atmosphere interaction alters possible icing conditions the most in January and February, with a
 422 maximum reduction by 153 hours (Table 3). At 20 m, wind plants cause a reduction by up to 157 hours in January
 423 and February. In each case, the reduction in possible freezing-icing conditions is spatially coincident with the wind
 424 plant areas (Figure 7). At the 138 m hub height, the change to the number of freezing-conditionsFSS hours also
 425 maximizes in DecemberJanuary and February, with a reduction by 96 hours.

426
 427 **Table 3. The maximum turbine-induced change in freezing-FSS hours by month and height.**

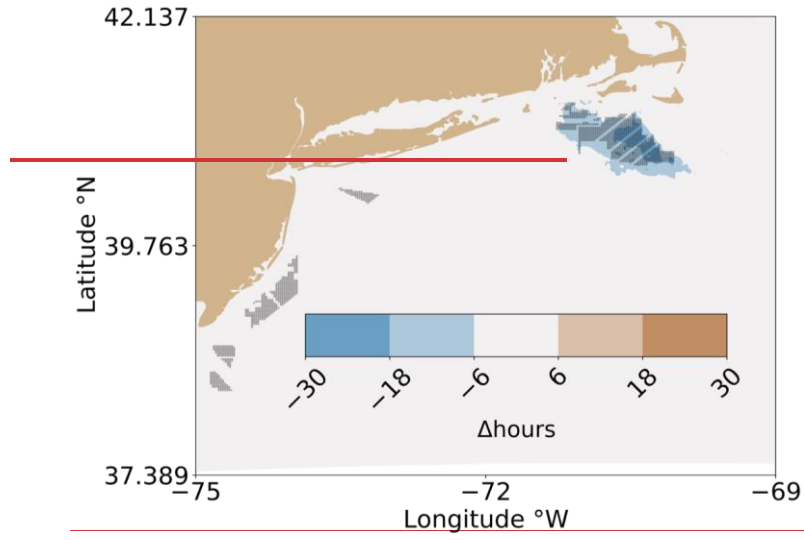
<u>Maximum cChange in Number of Freezing Hours Throughout Domain</u>						
	November	December	January	February	March	April
10 m	0	<u>-32</u>	<u>-143</u>	<u>-153</u>	<u>-110</u>	0
20 m	0	-4	<u>-157</u>	<u>-156</u>	-12	0
138 m	0	<u>-56</u>	<u>-93</u>	<u>-93</u>	<u>-53</u>	0

428
 429 The introduction of wind turbines also increases the chance for freezing surrounding the wind plants, reaching
 430 maxima in March of 5 and 6 hours at 10 m and 23 m, respectively (,). Flow acceleration is present adjacent to the

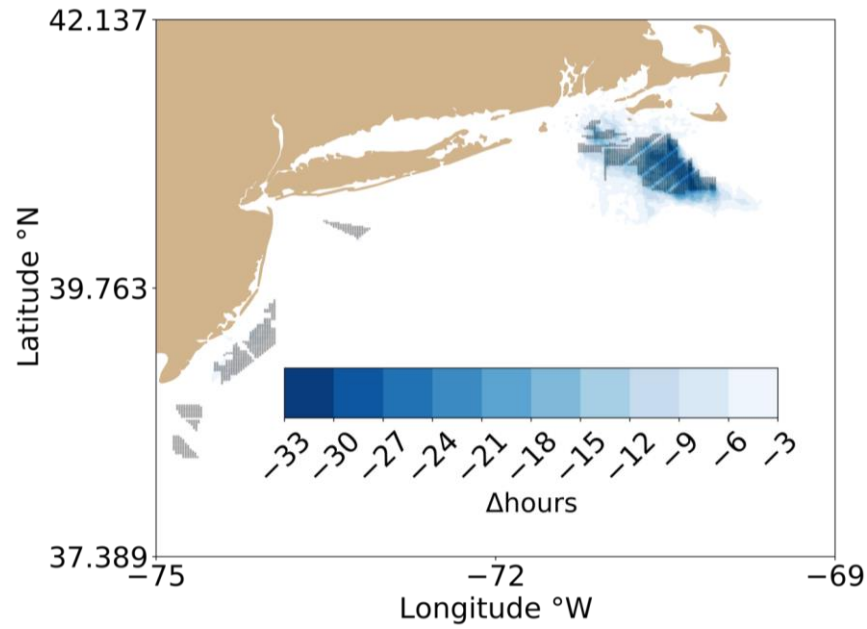
Formatted: Indent: First line: 0"

431 wake as winds deflect around the clusters (Stoelinga et al., 2022; Golbazi et al., 2022). However, freezing
432 enhancement is isolated to a speckled pattern (-), does not coincide with the wind speed enhancement, and thus may
433 result from numerical noise introduced by the WFP (Aneel et al., 2018; Lauridsen and Aneel, 2018). As
434 modifications to the percentage of freezing conditions at the hub height are not spatially coincident with the lease
435 areas or prevailing wind, these changes may also result from numerical noise (-).

436



437



438

439

440

Figure 7. The (WFP-NWF) change in ~~percentage number of freezing FSS~~ hours at 10 m November 2019 to March 2020. Blue contours indicate a ~~percentage reduction~~, and orange contours indicate a ~~percentage increase~~.

441
442 Overall, Similarly, the presence of wind turbines has a minimal impact to the number of hours FSS freezing
443 conditions occur by means of icing PPR at the POI. The duration of nonzero PPR over the November through March
444 winter period increases by 3 hours, or from 253 to 256 hours total, at a point centered on the RIMA block. The total
445 duration of CAO decreases by 1 hour does not change, or from 200 hours to 199 hours, after the installation of wind
446 plants and remains at 202 hours. The total number of events (seven) does not change in the presence of wind
447 turbines, and all flagged timestamps still cause light icing of less than 0.7 cm h⁻¹.

448 449 4 Conclusions

450 Herein, we assess the threat of freezing-icing conditions at 10 and 20 m due to freezing sea-spray icing and at
451 the hub-height riming due to precipitation and in-cloud icing on wind turbines. The simulation study encompasses
452 the mid-Atlantic Outer Continental Shelf based on a 210-year WRF dataset from 01 January 2000 to 31 December
453 2020 and another WRF dataset using year-long simulations from 01 September 2019 to 31 August 2020. In each
454 case, we focus on the wintertime period from November through March. We consider the present icing risk from
455 simulations with no wind farms (NOW-23, NWF) and assess the post-production-construction adjustments by
456 incorporating the effects of turbines (WFP) in a full buildout of the wind plant lease areas.

457
458 Using an FSS predictability equation (PR) We, we detect seven events flagged for freezing-sea-spray FSS
459 conditions in NWF with a total duration of 253 hours during the November 2019 to March 2020 period. All times
460 during the period with nonzero icing predictability (PPR) contain light ice accumulation of less than 0.7 cm h⁻¹,
461 which is typical for the region of the mid-Atlantic bight as assessed from 2000 to 2020. Centered at the RIMA block
462 of lease areas, six of the all seven events have an associated CAO in NWF during the 2019–2020 winter, and all
463 seven events have corresponding CAO at the northeast end of the block. In the NOW-23 dataset from November
464 2019 to March 2020 over the same period, eight total events are flagged, and all eight correspond with CAO. From
465 2000 to 2020 over the 21-year climatology, every CAO event has a corresponding freezing-sea-spray FSS event,
466 although not all freezing-FSS events have attendant CAO. Thus, offshore freezing-icing conditions may be forecast
467 with reasonable fidelity through accompanying CAO, although other drivers exist. There is strong teleconnection
468 between anomalous arctic sea level pressure sea level pressure and CAO, as 93 % of CAO events in the eastern U.S.
469 contained an antecedent positive arctic sea level pressure anomaly a week in advance (Vavrus et al., 2006).

470
471 The number of FSS hours Freezing conditions exhibit spatial variability, as assessed using our detection criteria
472 of low air sea surface temperatures and strong winds. The hazards intensify toward higher latitudes where air and
473 sea temperatures are colder and wind speeds are faster, near the land surface where cold air advects offshore, and by
474 Nantucket and the Long Island Sound where SSTs are colder. Freezing-Icing conditions at the hub height, as
475 assessed by low air temperatures and precipitation or saturated air, from supercooled liquid water are less more
476 frequent. The icing hazard is greatest during January when wind speeds are fast and temperatures are cold. At 10 m
477 in January, favorable conditions for icing occur up to 676 hours. At 20 m in January, the duration of icing conditions
478 increases is similar at 6870 hours. Finally, at the hub height, freezing-icing conditions occur for up to 11929 hours

479 ~~in the Gulf of Maine east of Cape Cod and pose no risk to the lease areas.~~ Overall, the 2019–2020 winter period is
480 the mildest winter when considering the 210-year ~~period~~ climatology. Although the 2019–2020 winter season has
481 the fewest number of ~~freezing-freezing sea spray~~ hours, all winters contain light ice accumulation rates of 0.7 cm
482 h⁻¹.

483
484 The introduction of large wind plants makes a small impact on the icing risk within the wind plant clusters. In
485 wintertime unstable conditions, which occur 64 % of the time from November 2019 through March 2020, wind
486 turbines introduce a mean near-surface cooling effect. Despite the enhanced freezing risk from supplementary
487 cooling, slower wind speeds in the wake mitigate the ~~icing~~ hazard. ~~A m~~Mean reductions in wind speeds within the
488 wakes reach ~~es~~ up to -0.57 m s^{-1} in unstable ~~conditions-stratification~~ with a ~~meann~~ introduction of cooler air up to
489 -0.041 K . As assessed using wind speed, air temperature, and SST criteria, the change in ~~icing-FSS~~ risk over the
490 2019–2020 wintertime period is a net reduction, by ~~up to only 153~~ hours at both 10 and 20 m. ~~At 20 m, mitigation~~
491 ~~reaches up to 17 hours.~~ The alleviation by slower wind speeds is largest within the RIMA block of wind plants
492 which contains the greatest number of turbines ~~and the greatest number of FSS hours relative to other wind energy~~
493 ~~areas.~~ When assessed using ~~icing~~ PPR centered on the RIMA block, the number of ~~icing~~ hours ~~increases by 3~~
494 ~~freezing conditions and with no change to CAO occur change by 3 and -1 hours, respectively hours.~~ ~~Although the~~
495 ~~2019 through 2020 winter period is the mildest winter, and thus not representative of the 21-year climatology of FSS~~
496 ~~conditions, this period captures well the post-construction effects of wind plants. We note that such effects may~~
497 ~~bc~~ However, the 2019 through 2020 winter period is the mildest winter, so the introduction of wind plants may make
498 more significant ~~changes during~~ during harsher winters.

499
500 Future OCS winter storm frequency may differ due to climate change. For instance, warming Arctic
501 temperatures, which reduce the meridional geopotential height gradient between the Arctic and midlatitudes, can
502 weaken the jet stream. Slower zonal winds and more pronounced Rossby waves amplify the transport of extreme
503 winter weather to the midlatitudes (Cohen et al., 2020). Future East Coast storm activity and temperature may
504 experience modulations based on large-scale teleconnections such as El Niño and the North Atlantic Oscillation
505 (Hall and Booth, 2017). Further, Arctic amplification may increase the strength of teleconnection found between
506 positive Arctic sea level pressure anomalies and CAO (Vavrus et al., 2006).

507
508 Finally, we assume that sea spray provides a consistent moisture flux at 10 and 20 m during fast wind
509 conditions, that the droplet size of spray is homogeneous, and that the number distribution by height is constant. ~~The~~
510 ~~impingement of waves onto offshore structures provides a larger source of moisture than wind-generated spray that~~
511 ~~is dependent on the wave height and wave period.~~ Future studies may benefit from coupling WRF with wave
512 models, such as Wave Watch III (Tolman et al., 2019) and Simulating WAVes Nearshore (SWAN Team, 2020) for
513 precise modeling of wave ~~induced-sea-spray~~ characteristics and ~~for~~ current dynamics, such as stratified cold pooling
514 around Cape Cod. New satellite methods are being developed to quantify occurrences of freezing sea spray (Line et
515 al., 2022), and future developments ~~cs~~ should compare the FSS criteria to satellite observations of FSS.

516

5 Code and data availability

517 The dataset and files that support this work are publicly available. The ERA5 initial and boundary conditions can be
518 downloaded from the ECMWF Climate Data Store at [https://cds.climate.copernicus.eu/cdsapp#!/dataset/reanalysis-
520 era5-pressure-levels?tab=form](https://cds.climate.copernicus.eu/cdsapp#!/dataset/reanalysis-
519 era5-pressure-levels?tab=form). Shapefiles including the bounds for wind energy lease areas are at
521 <https://www.boem.gov/renewable-energy/mapping-and-data/renewable-energy-gis-data>. Wind turbine coordinates
522 and their power and thrust curves are provided at <https://zenodo.org/record/7374283#.Y4YZxC-B1KM>. WRF
523 namelists for NWF and WFP simulations may be acquired from [https://zenodo.org/record/7374239#.Y4YaOy-
524 B1KM](https://zenodo.org/record/7374239#.Y4YaOy-
524 B1KM). The NOW-23 simulation output data are available in HDF5 format at <https://doi.org/10.25984/1821404>.

525

6 Author contributions

526 Conceptualization: JKL, MO. Resources: MO, NB. Methodology: DR, JKL. Software: DR. Formal analysis and
527 visualization: DR. Investigation: DR and JKL. Writing – original draft: DR and JKL. Writing – review and editing:
528 all co-authors. Supervision: JKL.

530

7 Competing interests

531 At least one of the (co-)authors is a member of the editorial board of Wind Energy Science. Furthermore, Mike
532 Optis co-authored the submitted manuscript while an employee of the National Renewable Energy Laboratory. He
533 has since founded Veer Renewables, which recently released a wind modeling product, WakeMap, which is based
534 on a similar numerical weather prediction modeling framework as the one described in this manuscript. Data from
535 WakeMap is sold to wind energy stakeholders for profit. Public content on WakeMap include a website (<http://www.veer.eco/wakemap/>),
536 a white paper ([https://veer.eco/wp-
537 content/uploads/2023/02/WakeMap_White_Paper_Veer_Renewables.pdf](https://veer.eco/wp-content/uploads/2023/02/WakeMap_White_Paper_Veer_Renewables.pdf)) and several LinkedIn posts promoting
538 WakeMap. Mike Optis is the founder and president of Veer Renewables, a for-profit consulting company. Mike
539 Optis is a shareholder of Veer Renewables and owns 92 % of its stock.

541

8 Acknowledgements

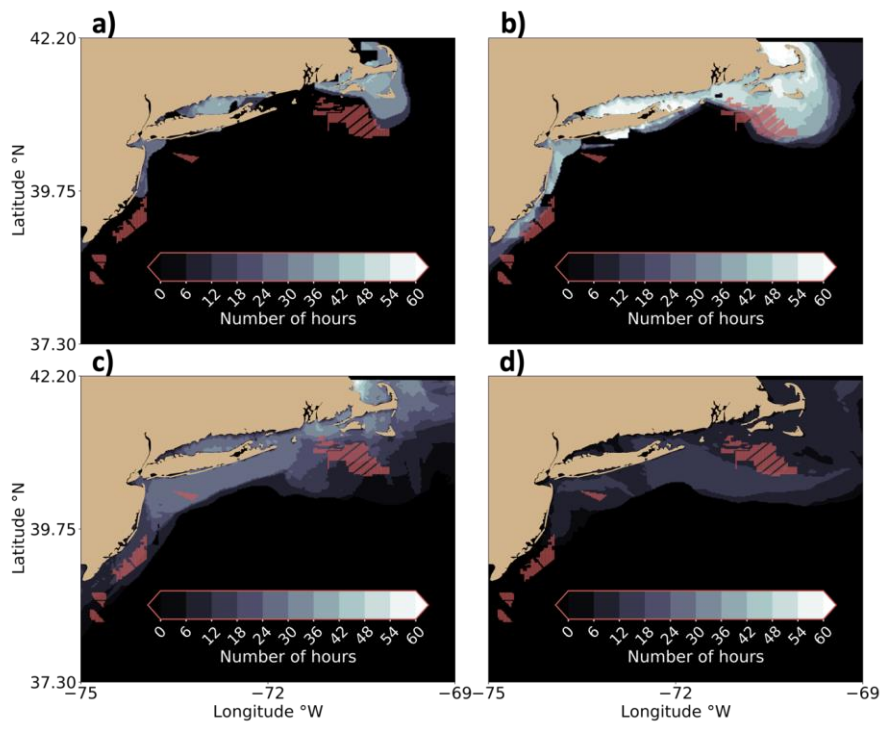
542 This work utilized the Alpine high-performance computing resource at the University of Colorado Boulder. Alpine
543 is jointly funded by the University of Colorado Boulder, the University of Colorado Anschutz, and Colorado State
544 University. Data storage supported by the University of Colorado Boulder ‘PetaLibrary’ A portion of this research
545 was performed using computational resources sponsored by the DOE’s Office of Energy Efficiency and Renewable
546 Energy and located at NREL. This work was authored in part by the National Renewable Energy Laboratory,
547 operated by Alliance for Sustainable Energy, LLC, for the US Department of Energy (DOE) under contract no. DE-
548 AC36-08GO28308. Funding was provided by the US Department of Energy Office of Energy Efficiency and
549 Renewable Energy Wind Energy Technologies Office. Support for the work was also provided by the National
550 Offshore Wind Research and Development Consortium under agreement no. CRD-19-16351. The views expressed
551 in the article do not necessarily represent the views of the DOE or the US Government. The US Government retains
552 and the publisher, by accepting the article for publication, acknowledges that the US Government retains a
553 nonexclusive, paid-up, irrevocable, worldwide license to publish or reproduce the published form of this work, or
554 allow others to do so, for US Government purposes.

556 The authors wish to thank Louis Bowers and Sarah McElman for their questions that led to this line of inquiry.

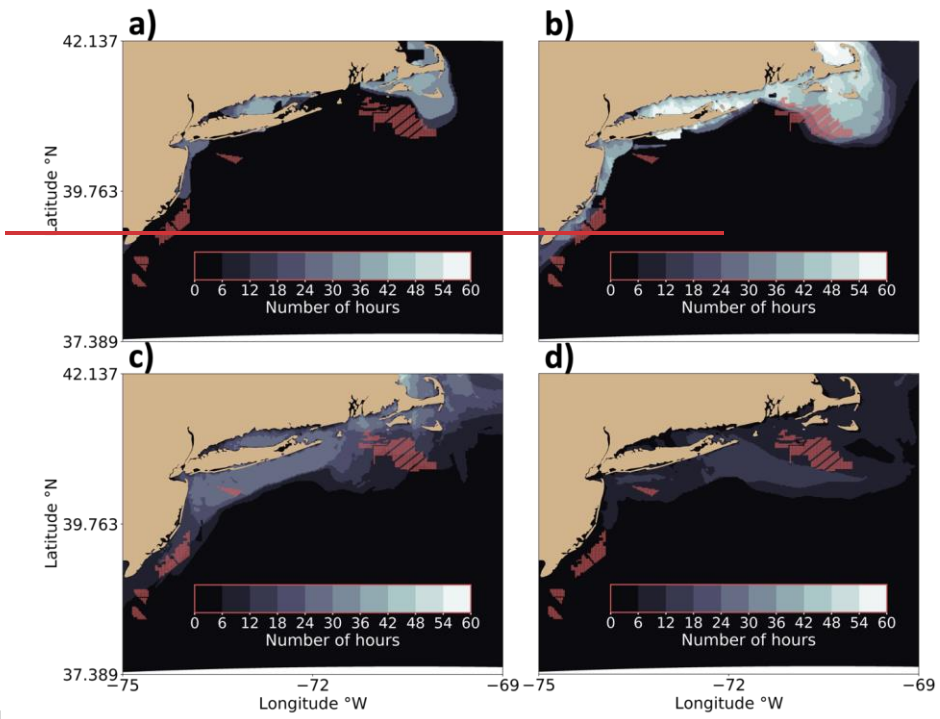
557

558 **9 Appendices**

559 **Appendix A**



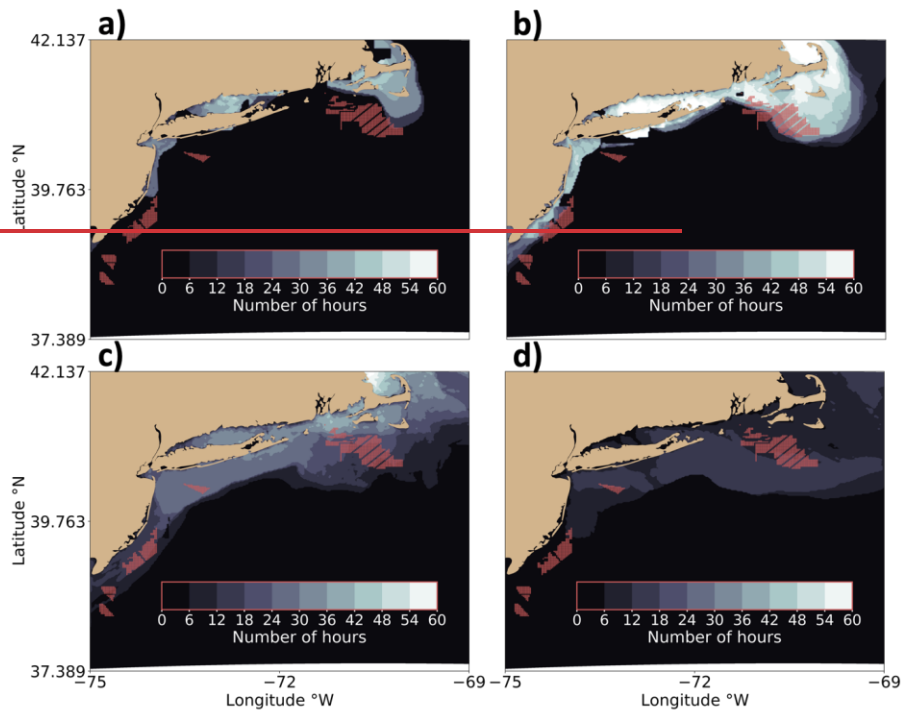
560



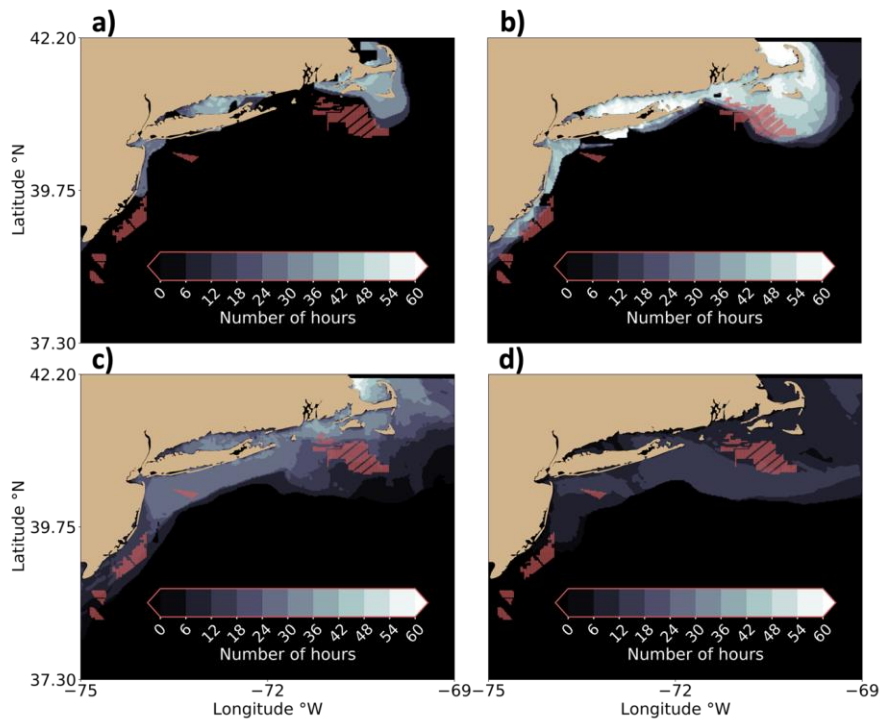
561

562 **Figure. A1.** The number of freezing hours at 10 m during (a) December 2019, (b) January 2020, (c) February 2020, and
 563 (d) March 2020. Lighter contouring indicates higher percentages. Red dots indicate turbine locations.

564

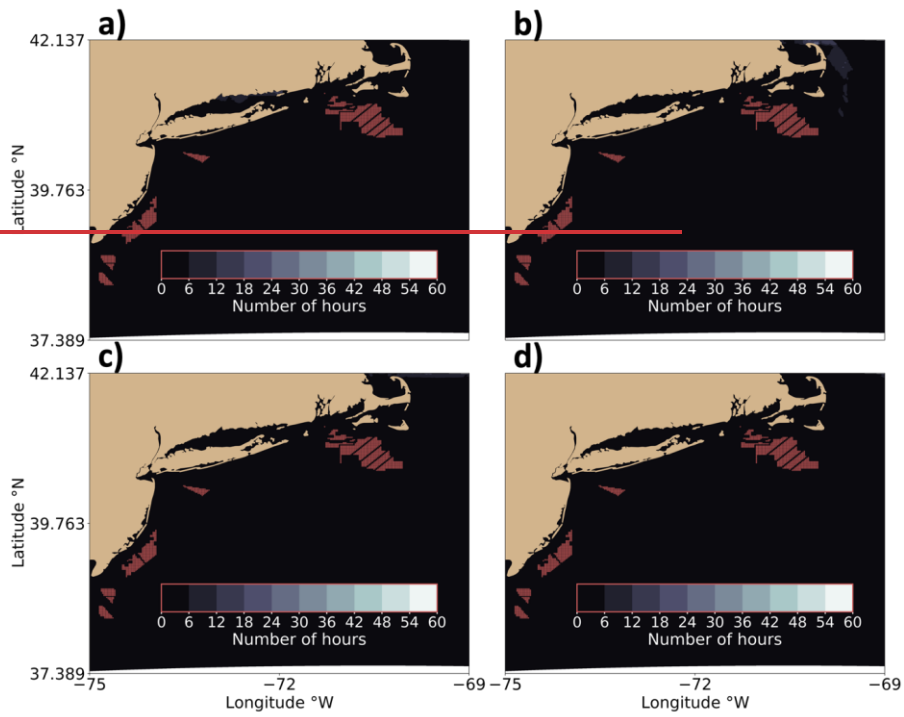


565

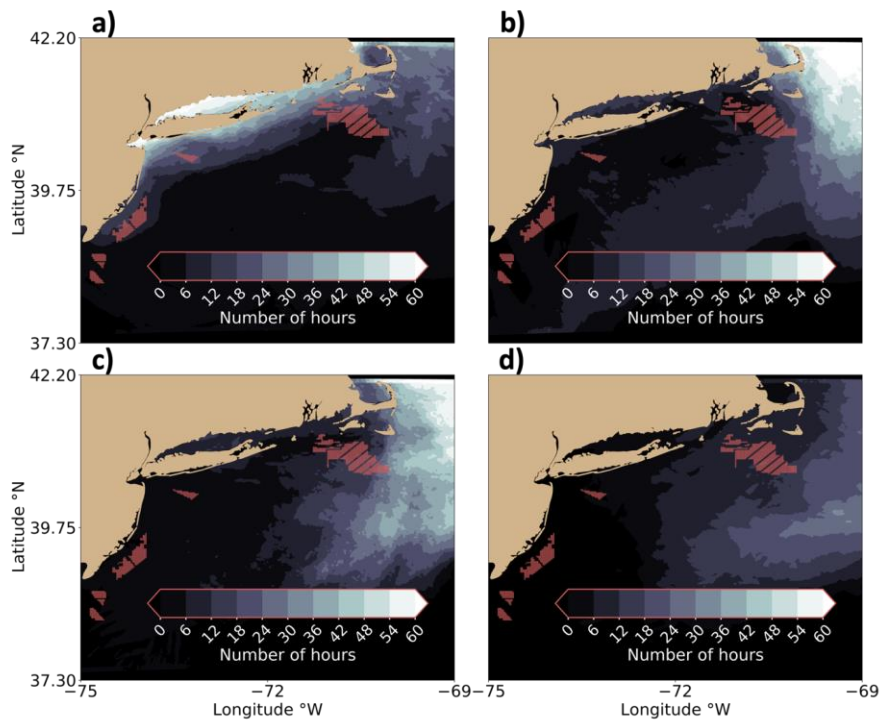


566
 567 **Figure A2.** The number of freezing hours at 20 m during (a) December 2019, (b) January 2020, (c) February 2020, and (d)
 568 March 2020. Lighter contouring indicates higher percentages. Red dots indicate turbine locations.

569



570



571

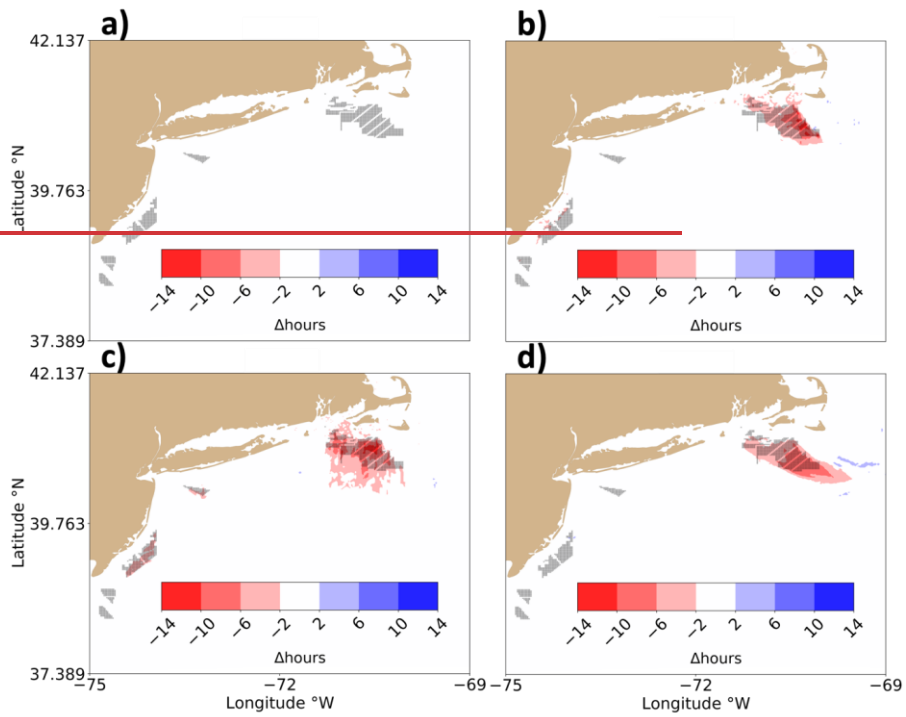
572

573

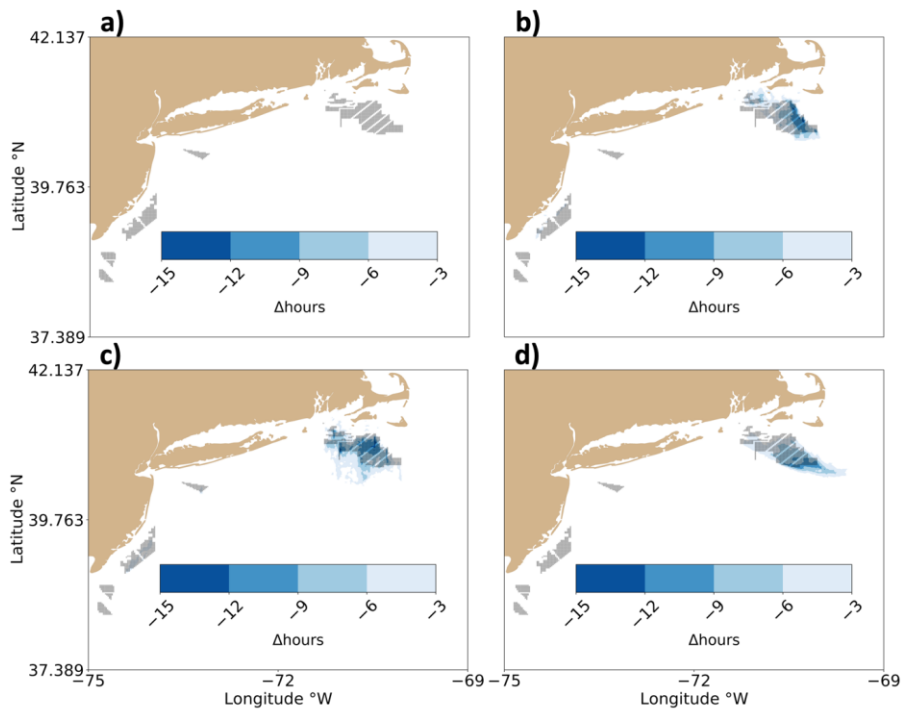
574

575

Figure A3. The number of freezing hours at hub height during (a) December 2019, (b) January 2020, (c) February 2020, and (d) March 2020. Lighter contouring indicates higher percentages. Note the color scheme is different from Supplementary Figs. 1 and 2. Red dots indicate turbine locations.



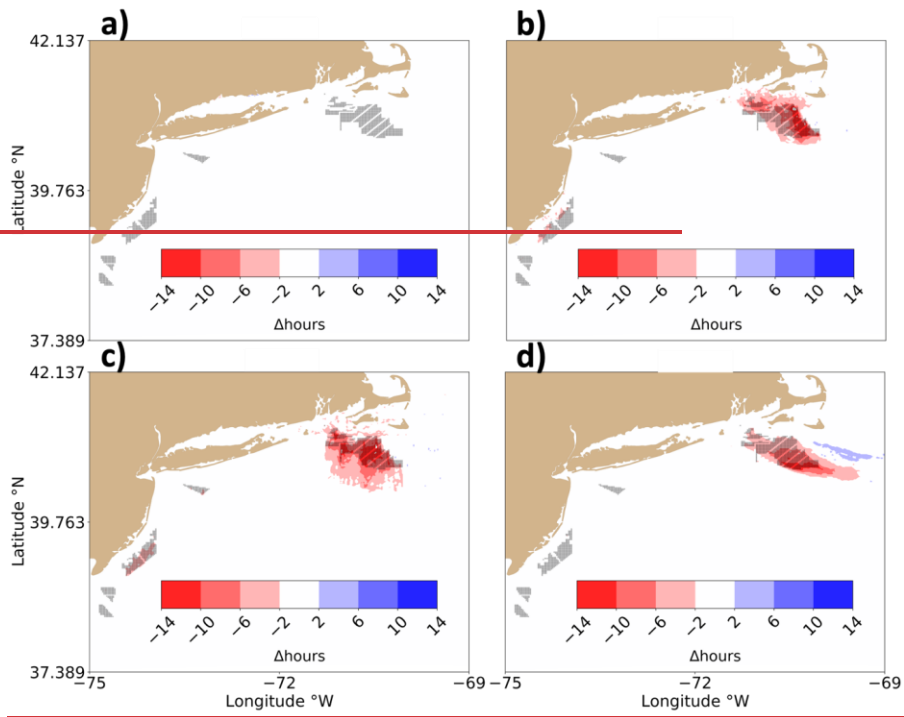
576



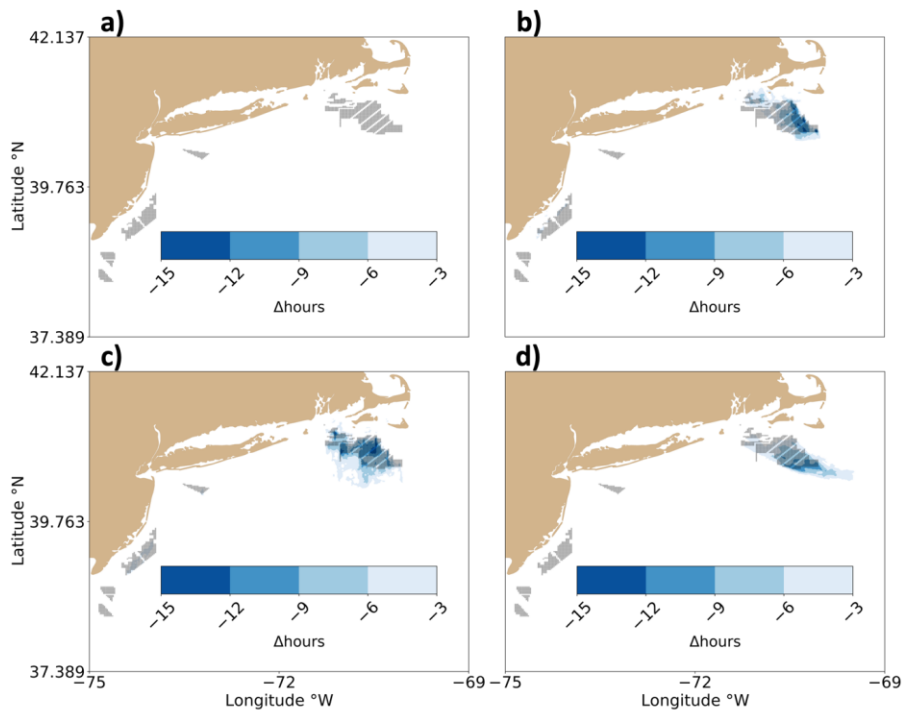
577

578 **Figure A4.** The (WFP-NWF) difference in freezing hours at 10 m during (a) December 2019, (b) January 2020, (c)
 579 February 2020, and (d) March 2020. Blue (red) contouring indicates higher-fewer hours(lower) percentages. Gray dots
 580 indicate turbine locations.

581



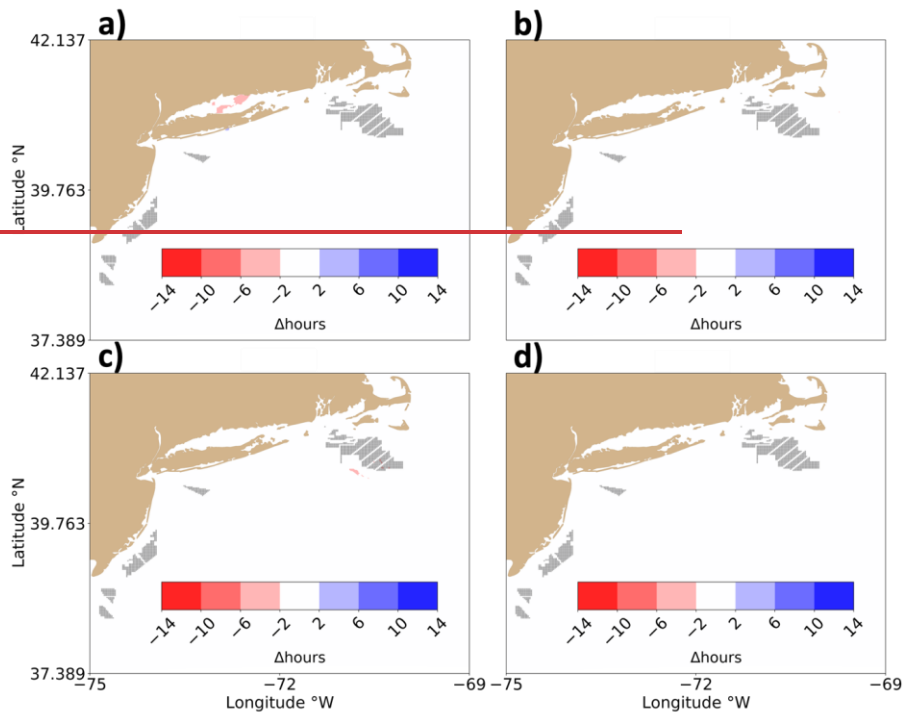
582



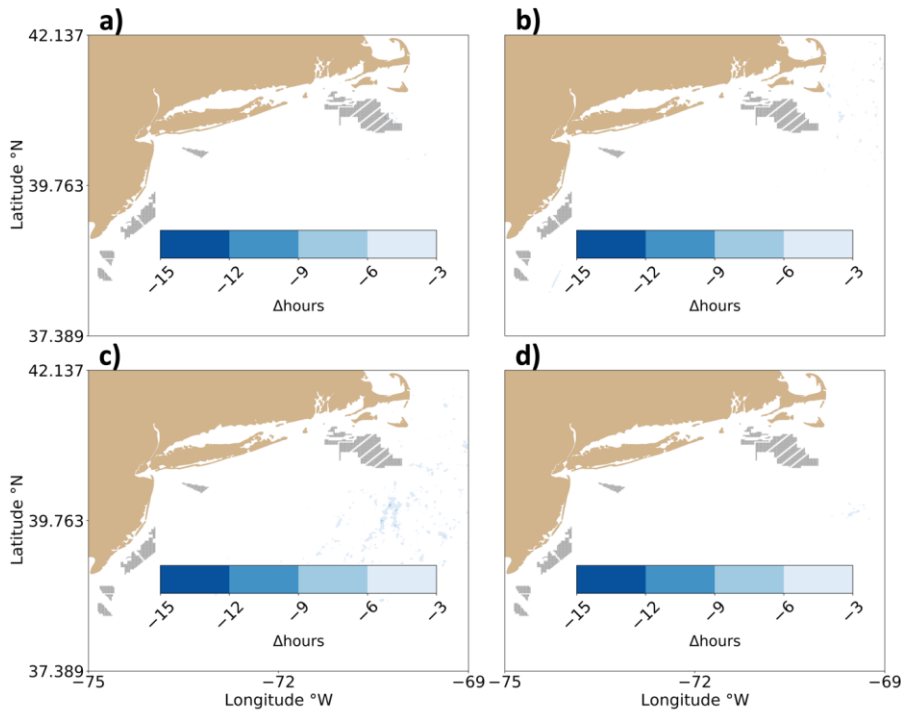
583

584 **Figure A5.** The (WFP_0-NWF) difference in freezing hours at 20 m during (a) December 2019, (b) January 2020, (c)
 585 February 2020, and (d) March 2020. **Blue contouring indicates fewer hours**Blue-(red) contouring indicates higher (lower)
 586 percentages. Gray dots indicate turbine locations.

587



588



589
 590 **Figure A6.** The (WFP-NWF) difference in freezing hours at the hub height during (a) December 2019, (b) January 2020,
 591 (c) February 2020, and (d) March 2020. **Blue contouring indicates fewer hours**Blue (red) contouring indicates higher
 592 (lower) percentages. Gray dots indicate turbine locations.

593 **Appendix B**

594 As discussed in Section 2.3, we detect FSS conditions using common thresholds for the meteorological
 595 conditions (Guest and Luke, 2005; Dehghani-Sanij et al., 2017; Line et al., 2022). These criteria require strong wind
 596 speeds greater than 9 m s^{-1} , cold air temperatures below -1.7° C , and cold SSTs less than 7° C . As reviewed by
 597 (Dehghani-Sanij et al., (2017), FSS conditions are promising when the air temperature is below either -1.7° C or
 598 -2° C to account for the lower freezing point of saline ocean water; the salt content of which determines this
 599 threshold. Although SST thresholds of 5° C or 7° C are prevalent, a threshold up to 8.9° C has been used (U.S.
 600 Navy, 1988). As such, we quantify some of the uncertainty by calculating the number of hours that FSS conditions
 601 occur using conservative thresholds, which produce fewer icing hours (FEWER), and liberal thresholds, which
 602 promote more icing hours (MORE) (Table B1). As there is wider agreement regarding the wind speed threshold
 603 (Dehghani-Sanij et al., 2017; Guest and Luke, 2005; Line et al., 2022; Ross and Cardone, 1974; Monahan et al.,
 604 1983; Monahan and MacNiocail, 1986), we hold it constant. Due to computational constraints, we only assess the
 605

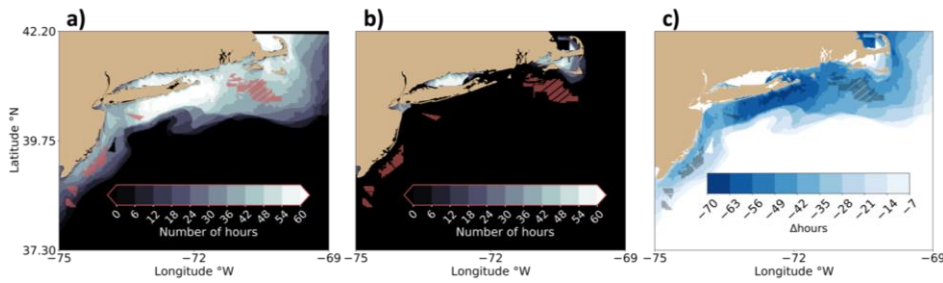
Formatted: Font: Bold
 Formatted: Indent: First line: 0.5"

606 number of icing hours throughout the domain at 10 m and during January 2020 because it has the greatest number of
 607 icing hours.

608 **Table B1. Icing detection criteria by sensitivity analysis type.**

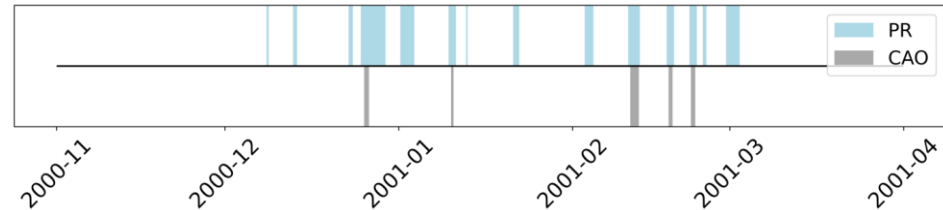
Acronym	Air temperature	Sea surface temperature	Wind speed
FEWER	$<-2^{\circ}\text{C}$	$<5^{\circ}\text{C}$	$>9\text{ m s}^{-1}$
MORE	$<-1.7^{\circ}\text{C}$	$<8.9^{\circ}\text{C}$	$>9\text{ m s}^{-1}$

610
 611 As expected, more conservative thresholds produce fewer FSS hours and vice versa (Fig. B1 a,b,c). In
 612 FEWER, the meteorological conditions conducive to icing maximize at 60 hours. Using more liberal criteria in
 613 MORE, the maximum number of hours increases to 67. Despite the small change in the maximum number of hours
 614 FSS occurs, the regional variation is large; the area covered by icing conditions increases from 8,924 km² to 135,244
 615 km² from FEWER to MORE, or roughly 15 times greater than FEWER, or 2.2 times greater than our production set
 616 of criteria. Regional variability follows SST patterns and only occurs in FEWER where the SST is relatively cold in
 617 the Long Island Sound and Nantucket Sound (Table B1b), as discussed previously.

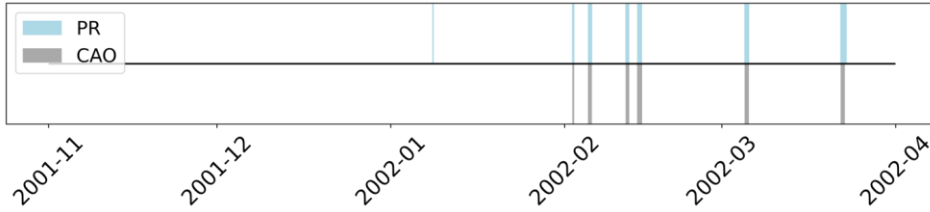


619
 620 **Fig. B1. The number of hours FSS conditions occur during January 2020 at 10 m in NWF using thresholds for (a)**
 621 **FEWER, (b) MORE, and (c) the (FEWER-MORE) difference. Lighter contouring indicates more freezing hours in (a)**
 622 **and (b). Darker blues represent a larger reduction in number of hours in (c). Turbine locations are shown as red dots in**
 623 **(a) and (b) and as black dots in (c).**

624 **Appendix C**



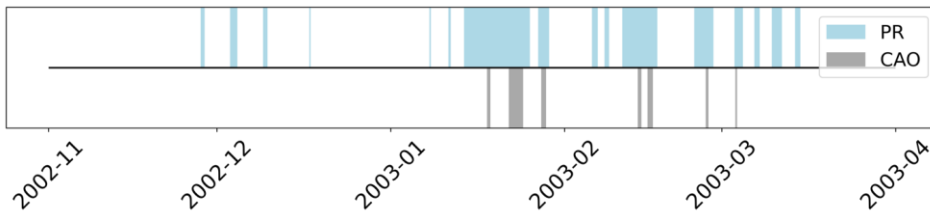
626
 627 **Fig. C1. Time series of CAO and FSS events from November 2000 to April 2001. Light-blue shading indicates the**
 628 **duration of nonzero PR and gray shading indicates the duration of detected CAO from NOW-23.**



Formatted: Keep with next

629
630
631

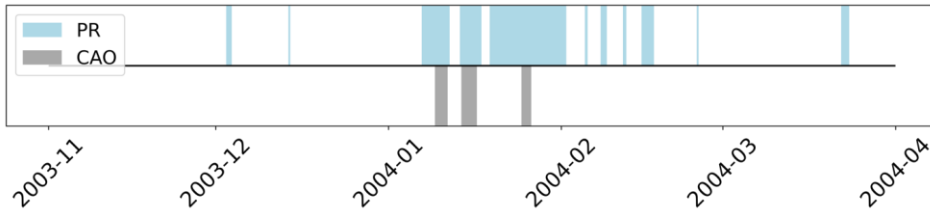
Fig. C2. Time series of CAO and FSS events from November 2001 to April 2002. Light-blue shading indicates the duration of nonzero PR and gray shading indicates the duration of detected CAO from NOW-23.



Formatted: Keep with next

632
633
634

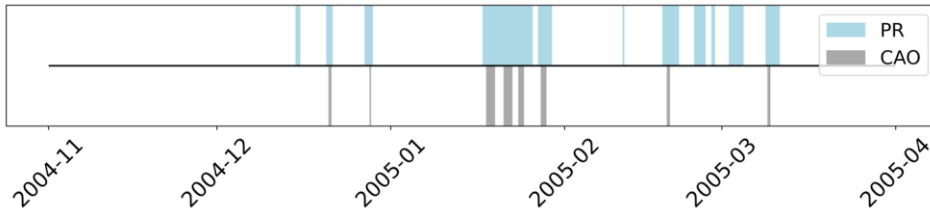
Fig. C3. Time series of CAO and FSS events from November 2002 to April 2003. Light-blue shading indicates the duration of nonzero PR and gray shading indicates the duration of detected CAO from NOW-23.



Formatted: Keep with next

635
636
637

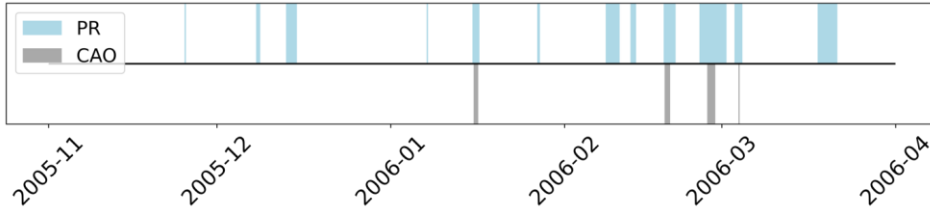
Fig. C4. Time series of CAO and FSS events from November 2003 to April 2004. Light-blue shading indicates the duration of nonzero PR and gray shading indicates the duration of detected CAO from NOW-23.



Formatted: Keep with next

638
639
640

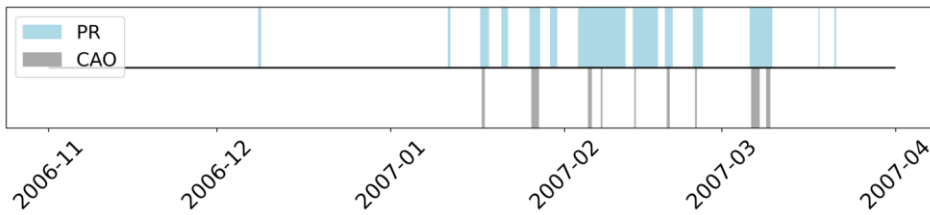
Fig. C5. Time series of CAO and FSS events from November 2004 to April 2005. Light-blue shading indicates the duration of nonzero PR and gray shading indicates the duration of detected CAO from NOW-23.



Formatted: Keep with next

641
642
643

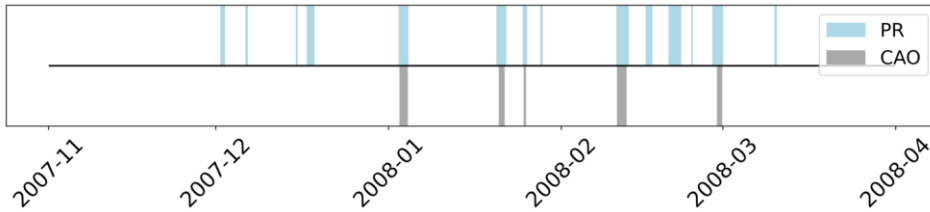
Fig. C6. Time series of CAO and FSS events from November 2005 to April 2006. Light-blue shading indicates the duration of nonzero PR and gray shading indicates the duration of detected CAO from NOW-23.



Formatted: Keep with next

644
645
646

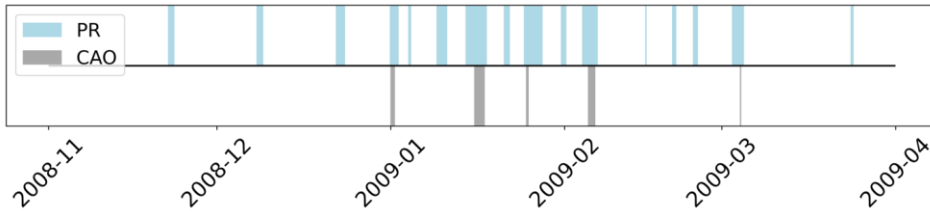
Fig. C7. Time series of CAO and FSS events from November 2006 to April 2007. Light-blue shading indicates the duration of nonzero PR and gray shading indicates the duration of detected CAO from NOW-23.



Formatted: Keep with next

647
648
649

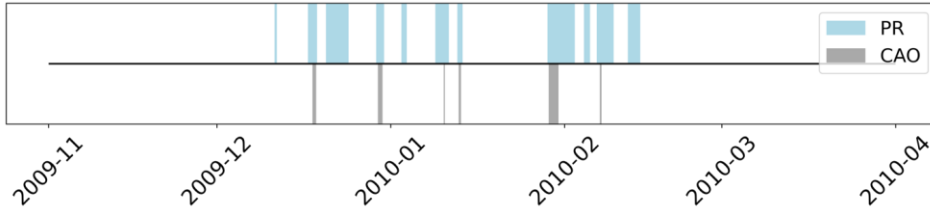
Fig. C8. Time series of CAO and FSS events from November 2007 to April 2008. Light-blue shading indicates the duration of nonzero PR and gray shading indicates the duration of detected CAO from NOW-23.



Formatted: Keep with next

650
651
652

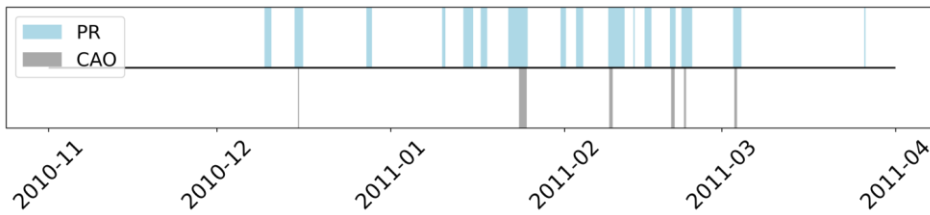
Fig. C9. Time series of CAO and FSS events from November 2008 to April 2009. Light-blue shading indicates the duration of nonzero PR and gray shading indicates the duration of detected CAO from NOW-23.



Formatted: Keep with next

653
654
655

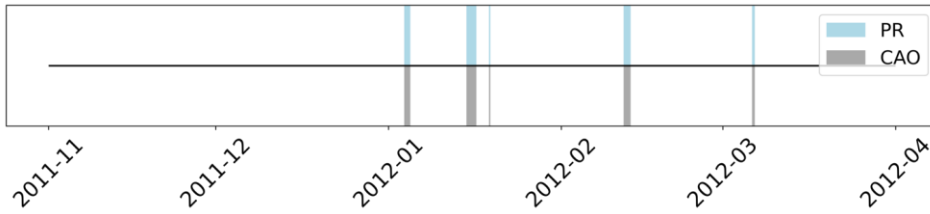
Fig. C10. Time series of CAO and FSS events from November 2009 to April 2010. Light-blue shading indicates the duration of nonzero PR and gray shading indicates the duration of detected CAO from NOW-23.



Formatted: Keep with next

656
657
658

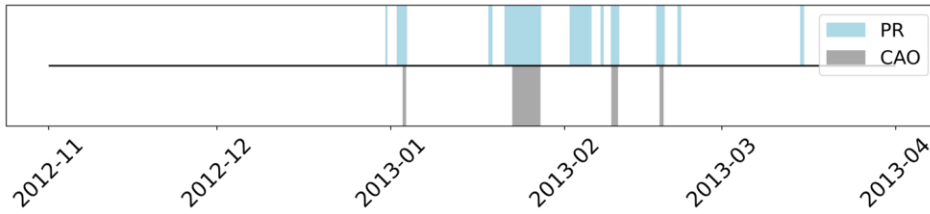
Fig. C11. Time series of CAO and FSS events from November 2010 to April 2011. Light-blue shading indicates the duration of nonzero PR and gray shading indicates the duration of detected CAO from NOW-23.



Formatted: Keep with next

659
660
661

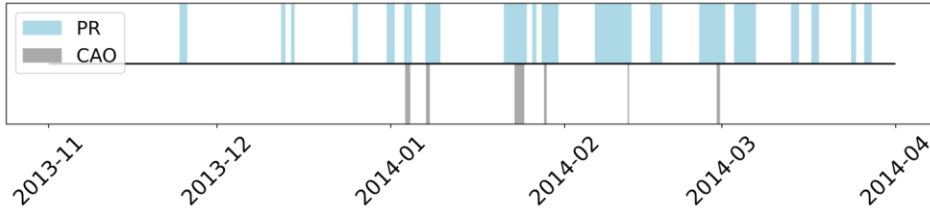
Fig. C12. Time series of CAO and FSS events from November 2011 to April 2012. Light-blue shading indicates the duration of nonzero PR and gray shading indicates the duration of detected CAO from NOW-23.



Formatted: Keep with next

662
663
664

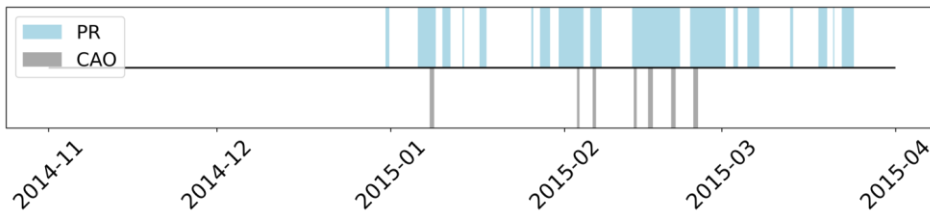
Fig. C13. Time series of CAO and FSS events from November 2012 to April 2013. Light-blue shading indicates the duration of nonzero PR and gray shading indicates the duration of detected CAO from NOW-23.



Formatted: Keep with next

665
666
667

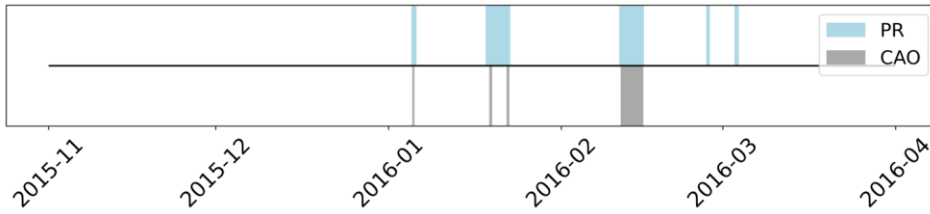
Fig. C14. Time series of CAO and FSS events from November 2013 to April 2014. Light-blue shading indicates the duration of nonzero PR and gray shading indicates the duration of detected CAO from NOW-23.



Formatted: Keep with next

668
669
670

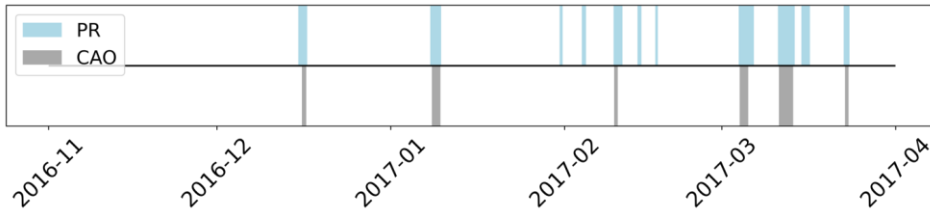
Fig. C15. Time series of CAO and FSS events from November 2014 to April 2015. Light-blue shading indicates the duration of nonzero PR and gray shading indicates the duration of detected CAO from NOW-23.



Formatted: Keep with next

671
672
673

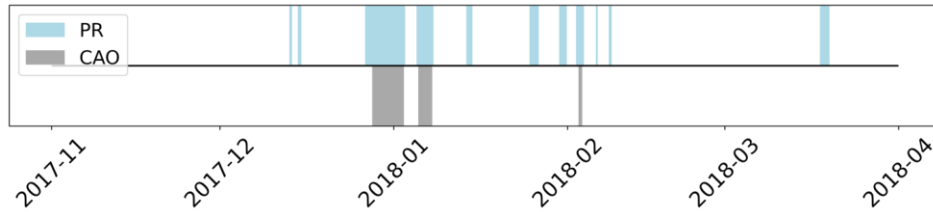
Fig. C16. Time series of CAO and FSS events from November 2015 to April 2016. Light-blue shading indicates the duration of nonzero PR and gray shading indicates the duration of detected CAO from NOW-23.



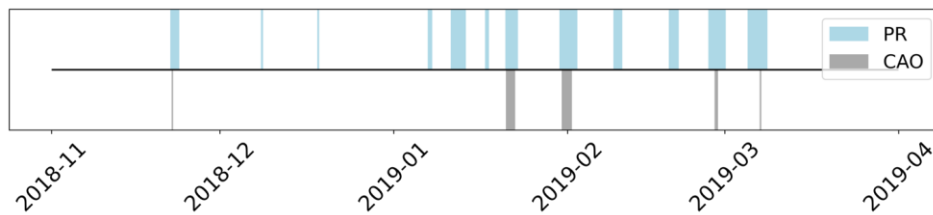
Formatted: Keep with next

674
675
676

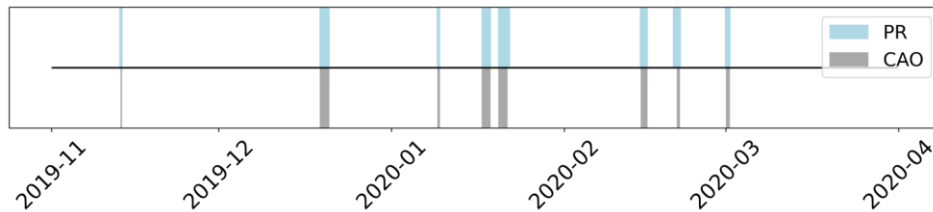
Fig. C17. Time series of CAO and FSS events from November 2016 to April 2017. Light-blue shading indicates the duration of nonzero PR and gray shading indicates the duration of detected CAO from NOW-23.



677 **Fig. C18.** Time series of CAO and FSS events from November 2017 to April 2018. Light-blue shading indicates the
 678 duration of nonzero PR and gray shading indicates the duration of detected CAO from NOW-23.
 679



680 **Fig. C19.** Time series of CAO and FSS events from November 2018 to April 2019. Light-blue shading indicates the
 681 duration of nonzero PR and gray shading indicates the duration of detected CAO from NOW-23.
 682



683 **Fig. C20.** Time series of CAO and FSS events from November 2019 to April 2020. Light-blue shading indicates the
 684 duration of nonzero PR and gray shading indicates the duration of detected CAO from NOW-23.
 685

686 **10 References**

687 **10**

688 Alexander, M. and Scott, J.: The influence of ENSO on air-sea interaction in the Atlantic, *Geophysical Research*
 689 *Letters*, 29, 46-1-46-4, <https://doi.org/10.1029/2001GL014347>, 2002.

691 Archer, C. L., Colle, B. A., Veron, D. L., Veron, F., and Sienkiewicz, M. J.: On the predominance of unstable
 692 atmospheric conditions in the marine boundary layer offshore of the U.S. northeastern coast, *Journal of Geophysical*
 693 *Research: Atmospheres*, 121, 8869–8885, <https://doi.org/10.1002/2016JD024896>, 2016.

694 Archer, C. L., Wu, S., Ma, Y., and Jiménez, P. A.: Two Corrections for Turbulent Kinetic Energy Generated by
 695 Wind Farms in the WRF Model, *Monthly Weather Review*, 148, 4823–4835, <https://doi.org/10.1175/MWR-D-20-0097.1>, 2020.

697 Atkinson, B. W. and Wu Zhang, J.: Mesoscale shallow convection in the atmosphere, *Reviews of Geophysics*, 34,
 698 403–431, <https://doi.org/10.1029/96RG02623>, 1996.

699 Battisti, L., Fedrizzi, R., Brighenti, A., and Laakso, T.: Sea ice and icing risk for offshore wind turbines,
 700 *Proceedings of the OWEMES*, 20–22,

Formatted: Keep with next

Formatted: Keep with next

Formatted: Keep with next

Formatted: Caption

Formatted: Normal

701 <https://citeseerx.ist.psu.edu/document?repid=rep1&type=pdf&doi=8bb110a8c86abf785b1b019dcc37150f09de90ae>,
702 2006.

703 Beiter, P., Musial, W., Duffy, P., Cooperman, A., Shields, M., Heimiller, D., and Optis, M.: The Cost of Floating
704 Offshore Wind Energy in California Between 2019 and 2032, [NREL/TP-5000-77384](https://doi.org/10.2172/1710181),
705 <https://doi.org/10.2172/1710181>, 2020.

706 Bodini, N., Lundquist, J. K., and Kirincich, A.: U.S. East Coast Lidar Measurements Show Offshore Wind Turbines
707 Will Encounter Very Low Atmospheric Turbulence, *Geophysical Research Letters*, 46, 5582–5591,
708 <https://doi.org/10.1029/2019GL082636>, 2019.

709 Bodini, N., Optis, M., Redfern, S., Rosencrans, D., Rybchuk, A., Lundquist, J. K., Pronk, V., Castagneri, S.,
710 Purkayastha, A., Draxl, C., Krishnamurthy, R., Young, E., Roberts, B., Rosenlieb, E., and Musial, W.: The 2023
711 National Offshore Wind data set (NOW-23), *Earth System Science Data*, 16, 1965–2006,
712 <https://doi.org/10.5194/essd-16-1965-2024>, 2024.

713 Chapman, D. C., Barth, J. A., Beardsley, R. C., and Fairbanks, R. G.: On the Continuity of Mean Flow between the
714 Scotian Shelf and the Middle Atlantic Bight, *Journal of Physical Oceanography*, 16, 758–772,
715 [https://doi.org/10.1175/1520-0485\(1986\)016<0758:OTCOMF>2.0.CO;2](https://doi.org/10.1175/1520-0485(1986)016<0758:OTCOMF>2.0.CO;2), 1986.

716 Cohen, J., Zhang, X., Francis, J., Jung, T., Kwok, R., Overland, J., Ballinger, T. J., Bhatt, U. S., Chen, H. W.,
717 Coumou, D., Feldstein, S., Gu, H., Handorf, D., Henderson, G., Ionita, M., Kretschmer, M., Laliberte, F., Lee, S.,
718 Linderholm, H. W., Maslowski, W., Peings, Y., Pfeiffer, K., Rigor, I., Semmler, T., Stroeve, J., Taylor, P. C.,
719 Vavrus, S., Vihma, T., Wang, S., Wendisch, M., Wu, Y., and Yoon, J.: Divergent consensus on Arctic
720 amplification influence on midlatitude severe winter weather, *Nat. Clim. Chang.*, 10, 20–29,
721 <https://doi.org/10.1038/s41558-019-0662-y>, 2020.

722 Contreras Montoya, L. T., Lain, S., and Ilinca, A.: A Review on the Estimation of Power Loss Due to Icing in Wind
723 Turbines, *Energies*, 15, 1083, <https://doi.org/10.3390/en15031083>, 2022.

724 Dehghani-Sanij, A. R., Dehghani, S. R., Naterer, G. F., and Muzychka, Y. S.: Sea spray icing phenomena on marine
725 vessels and offshore structures: Review and formulation, *Ocean Engineering*, 132, 25–39,
726 <https://doi.org/10.1016/j.oceaneng.2017.01.016>, 2017.

727 Donlon, C. J., Martin, M., Stark, J., Roberts-Jones, J., Fiedler, E., and Wimmer, W.: The Operational Sea Surface
728 Temperature and Sea Ice Analysis (OSTIA) system, *Remote Sensing of Environment*, 116, 140–158,
729 <https://doi.org/10.1016/j.rse.2010.10.017>, 2012.

730 Ferrel, W.: *Nashville Journal of Medicine and Surgery*, 11, 7–19,
731 <https://empslocal.ex.ac.uk/people/staff/gv219/classics.d/ferrel-nashville56.pdf>, 1856.

732 Ferrier, B. S., Jin, Y., Lin, Y., Black, T., Rogers, E., and DiMego, G.: Implementation of a new grid-scale cloud and
733 precipitation scheme in the NCEP Eta model, *Amer. Meteor. Soc. Conf. on Weather Analysis and Forecasting*, 19,
734 [https://scholar.google.com/scholar?hl=en&as_sdt=0%2C6&q=Implementation+of+a+new+grid-](https://scholar.google.com/scholar?hl=en&as_sdt=0%2C6&q=Implementation+of+a+new+grid-scale+cloud+and+precipitation+scheme+in+the+NCEP+Eta+model&btnG=)
735 [scale+cloud+and+precipitation+scheme+in+the+NCEP+Eta+model&btnG=](https://scholar.google.com/scholar?hl=en&as_sdt=0%2C6&q=Implementation+of+a+new+grid-scale+cloud+and+precipitation+scheme+in+the+NCEP+Eta+model&btnG=), 2002.

736 Fitch, A. C., Olson, J. B., Lundquist, J. K., Dudhia, J., Gupta, A. K., Michalakes, J., and Barstad, I.: Local and
737 Mesoscale Impacts of Wind Farms as Parameterized in a Mesoscale NWP Model, *Monthly Weather Review*, 140,
738 3017–3038, <https://doi.org/10.1175/MWR-D-11-00352.1>, 2012.

739 Fitch, A. C., Lundquist, J. K., and Olson, J. B.: Mesoscale Influences of Wind Farms throughout a Diurnal Cycle,
740 *Mon. Wea. Rev.*, 141, 2173–2198, <https://doi.org/10.1175/MWR-D-12-00185.1>, 2013.

741 Gao, L. and Hong, J.: Wind turbine performance in natural icing environments: A field characterization, *Cold*
742 *Regions Science and Technology*, 181, 103193, <https://doi.org/10.1016/j.coldregions.2020.103193>, 2021.

743 Gao, L. and Hu, H.: Wind turbine icing characteristics and icing-induced power losses to utility-scale wind turbines,
744 Proceedings of the National Academy of Sciences, 118, e2111461118, <https://doi.org/10.1073/pnas.2111461118>,
745 2021.

746 Geerts, B., Giangrande, S. E., McFarquhar, G. M., Xue, L., Abel, S. J., Comstock, J. M., Crewell, S., DeMott, P. J.,
747 Ebell, K., Field, P., Hill, T. C. J., Hunzinger, A., Jensen, M. P., Johnson, K. L., Juliano, T. W., Kollias, P., Kosovic,
748 B., Lackner, C., Luke, E., Lüpkes, C., Matthews, A. A., Neggens, R., Ovchinnikov, M., Powers, H., Shupe, M. D.,
749 Spengler, T., Swanson, B. E., Tjernström, M., Theisen, A. K., Wales, N. A., Wang, Y., Wendisch, M., and Wu, P.:
750 The COMBLE Campaign: A Study of Marine Boundary Layer Clouds in Arctic Cold-Air Outbreaks, Bulletin of the
751 American Meteorological Society, 103, E1371–E1389, <https://doi.org/10.1175/BAMS-D-21-0044.1>, 2022.

752 Golbazi, M., Archer, C. L., and Alessandrini, S.: Surface impacts of large offshore wind farms, Environ. Res. Lett.,
753 17, 064021, <https://doi.org/10.1088/1748-9326/ac6e49>, 2022.

754 Gómez, B. and Miguez-Macho, G.: The impact of wave number selection and spin-up time in spectral nudging,
755 Quarterly Journal of the Royal Meteorological Society, 143, 1772–1786, <https://doi.org/10.1002/qj.3032>, 2017.

756 Gryning, S.-E., Batchvarova, E., Brümmner, B., Jørgensen, H., and Larsen, S.: On the extension of the wind profile
757 over homogeneous terrain beyond the surface boundary layer, Boundary-Layer Meteorol, 124, 251–268,
758 <https://doi.org/10.1007/s10546-007-9166-9>, 2007.

759 Guest, P. and Luke, R.: The Power of Wind and Water, Mariners Weather Log,
760 https://www.vos.noaa.gov/MWL/dec_05/ves.shtml, 2005.

761 Hall, T. and Booth, J. F.: SynthETC: A Statistical Model for Severe Winter Storm Hazard on Eastern North
762 America, Journal of Climate, 30, 5329–5343, <https://doi.org/10.1175/JCLI-D-16-0711.1>, 2017.

763 Hersbach, H., Bell, B., Berrisford, P., Hirahara, S., Horányi, A., Muñoz-Sabater, J., Nicolas, J., Peubey, C., Radu,
764 R., Schepers, D., Simmons, A., Soci, C., Abdalla, S., Abellan, X., Balsamo, G., Bechtold, P., Biavati, G., Bidlot, J.,
765 Bonavita, M., De Chiara, G., Dahlgren, P., Dee, D., Diamantakis, M., Dragani, R., Flemming, J., Forbes, R.,
766 Fuentes, M., Geer, A., Haimberger, L., Healy, S., Hogan, R. J., Hólm, E., Janisková, M., Keeley, S., Laloyaux, P.,
767 Lopez, P., Lupu, C., Radnoti, G., de Rosnay, P., Rozum, I., Vamborg, F., Villaume, S., and Thépaut, J.-N.: The
768 ERA5 global reanalysis, Quarterly Journal of the Royal Meteorological Society, 146, 1999–2049,
769 <https://doi.org/10.1002/qj.3803>, 2020.

770 Hirsch, R. M., Slack, J. R., and Smith, R. A.: Techniques of trend analysis for monthly water quality data, Water
771 Resources Research, <https://doi.org/10.1029/WR018i001p00107>, 1982.

772 Hussain, M. M. and Mahmud, I.: pyMannKendall: a python package for non parametric Mann Kendall family of
773 trend tests., Journal of Open Source Software, 4, 1556, <https://doi.org/10.21105/joss.01556>, 2019.

774 Iacono, M. J., Delamere, J. S., Mlawer, E. J., Shephard, M. W., Clough, S. A., and Collins, W. D.: Radiative forcing
775 by long-lived greenhouse gases: Calculations with the AER radiative transfer models, Journal of Geophysical
776 Research: Atmospheres, 113, <https://doi.org/10.1029/2008JD009944>, 2008.

777 IEA: Available Technologies for Wind Energy in Cold Climates – report, [https://iea-wind.org/wp-](https://iea-wind.org/wp-content/uploads/2021/09/Lehtomaki-et-al.-2018-Available-Technologies-for-Wind-Energy-in-Cold-Climates-report-2-nd-edition-2018.pdf)
778 [content/uploads/2021/09/Lehtomaki-et-al.-2018-Available-Technologies-for-Wind-Energy-in-Cold-Climates-report-](https://iea-wind.org/wp-content/uploads/2021/09/Lehtomaki-et-al.-2018-Available-Technologies-for-Wind-Energy-in-Cold-Climates-report-2-nd-edition-2018.pdf)
779 [2-nd-edition-2018.pdf](https://iea-wind.org/wp-content/uploads/2021/09/Lehtomaki-et-al.-2018-Available-Technologies-for-Wind-Energy-in-Cold-Climates-report-2-nd-edition-2018.pdf), 2018.

780 ISO: Atmospheric Icing of Structures, Geneva, Switzerland, [ISO-12494:2017](https://cdn.standards.iteh.ai/samples/72443/2fb2033c3f844304b66281607516ec58/ISO-12494-2017.pdf),
781 <https://cdn.standards.iteh.ai/samples/72443/2fb2033c3f844304b66281607516ec58/ISO-12494-2017.pdf>, 2017.

782 Kain, J. S.: The Kain–Fritsch Convective Parameterization: An Update, Journal of Applied Meteorology and
783 Climatology, 43, 170–181, [https://doi.org/10.1175/1520-0450\(2004\)043<0170:TKCPAU>2.0.CO;2](https://doi.org/10.1175/1520-0450(2004)043<0170:TKCPAU>2.0.CO;2), 2004.

784 [Kraegel, L.](#): Destination likely sank after accumulating ice in heavy freezing spray, report says:
785 [https://www.ktoo.org/2018/07/16/destination-likely-sank-after-accumulating-ice-in-heavy-freezing-spray-report-](https://www.ktoo.org/2018/07/16/destination-likely-sank-after-accumulating-ice-in-heavy-freezing-spray-report-says/)
786 [says/](https://www.ktoo.org/2018/07/16/destination-likely-sank-after-accumulating-ice-in-heavy-freezing-spray-report-says/), last access: 12 April 2023.

787 Kraj, A. G. and Bibeau, E. L.: Phases of icing on wind turbine blades characterized by ice accumulation, *Renewable*
788 *Energy*, 35, 966–972, <https://doi.org/10.1016/j.renene.2009.09.013>, 2010.

789 Line, W. E., Grasso, L., Hillger, D., Dierking, C., Jacobs, A., and Shea, S.: Using NOAA Satellite Imagery to Detect
790 and Track Hazardous Sea Spray in the High Latitudes, *Weather and Forecasting*, 37, 351–369,
791 <https://doi.org/10.1175/WAF-D-21-0137.1>, 2022.

792 [NTSB](#): NTSB announces the probable cause of the sunken Scandies Rose:
793 <https://www.alaskasnewsresource.com/2021/06/29/ntsb-announce-probable-cause-sunken-scandies-rose/>, last access:
794 12 April 2023.

795 Madi, E., Pope, K., Huang, W., and Iqbal, T.: A review of integrating ice detection and mitigation for wind turbine
796 blades, *Renewable and Sustainable Energy Reviews*, 103, 269–281, <https://doi.org/10.1016/j.rser.2018.12.019>,
797 2019.

798 Martini, F., Contreras Montoya, L. T., and Ilinca, A.: Review of Wind Turbine Icing Modelling Approaches,
799 *Energies*, 14, 5207, <https://doi.org/10.3390/en14165207>, 2021.

800 Monahan, E. C. and MacNiocaill, G.: Oceanic Whitecaps And Their Role in Air-Sea Exchange Processes, D Reidel
801 Publishing Company, [e-ISBN-13: 978-94-009-4668-2](https://doi.org/10.1007/978-94-009-4668-2), <https://link.springer.com/book/10.1007/978-94-009-4668-2>,
802 1986.

803 Monahan, E. C., Fairall, C. W., Davidson, K. L., and Boyle, P. J.: Observed inter-relations between 10m winds,
804 ocean whitecaps and marine aerosols, *Quarterly Journal of the Royal Meteorological Society*, 109, 379–392,
805 <https://doi.org/10.1002/qj.49710946010>, 1983.

806 Monin, A. S. and Obukhov, A. M.: Basic laws of turbulent mixing in the surface layer of the atmosphere, *Tr. Akad.*
807 *Nauk SSSR Geophys. Inst.*, 24, 30, https://gibbs.science/efd/handouts/monin_obukhov_1954.pdf, 1954.

808 Musial, W., Spitsen, P., Duffy, P., Beiter, P., Marquis, M., Hammond, R., and Shields, M.: Offshore Wind Market
809 Report: 2022 Edition, [NREL/TP-5000-83544](https://www.nrel.gov/docs/fy22/tp-5000-83544.pdf), National Renewable Energy Laboratory, Golden, CO (United States),
810 <https://doi.org/10.2172/188338>, 2022.

811 Nakanishi, M. and Niino, H.: An Improved Mellor–Yamada Level-3 Model: Its Numerical Stability and Application
812 to a Regional Prediction of Advection Fog, *Boundary-Layer Meteorol.*, 119, 397–407,
813 <https://doi.org/10.1007/s10546-005-9030-8>, 2006.

814 [Nilsen, T.](#): Icing believed to cause sinking of fishing boat in Barents Sea, 17 missing:
815 <https://thebarentsobserver.com/en/2020/12/icing-believed-cause-sinking-fishing-boat-barents-sea-17-missing>, last
816 access: 12 April 2023.

817 Niu, G.-Y., Yang, Z.-L., Mitchell, K. E., Chen, F., Ek, M. B., Barlage, M., Kumar, A., Manning, K., Niyogi, D.,
818 Rosero, E., Tewari, M., and Xia, Y.: The community Noah land surface model with multiparameterization options
819 (Noah-MP): 1. Model description and evaluation with local-scale measurements, *Journal of Geophysical Research:*
820 *Atmospheres*, 116, <https://doi.org/10.1029/2010JD015139>, 2011.

821 Novacheck, J., Sharp, J., Schwarz, M., Donohoo-Vallett, P., Tzavelis, Z., Buster, G., and Rossol, M.: The Evolving
822 Role of Extreme Weather Events in the U.S. Power System with High Levels of Variable Renewable Energy,
823 *NREL/TP-6A20-78394*, 1837959, MainId:32311, *NREL/TP-6A20-78394*, 1837959, MainId:32311,
824 <https://doi.org/10.2172/1837959>, 2021.

825 NREL: 2023 National Offshore Wind data set (NOW-23), <https://dx.doi.org/10.25984/1821404>, 2020.

826 Glossary - NOAA's National Weather Service: <https://w1.weather.gov/glossary/index.php?word=freezing+spray>,
827 last access: 12 April 2023.

828 Nygaard, N. G.: Wakes in very large wind farms and the effect of neighbouring wind farms, *J. Phys.: Conf. Ser.*,
829 524, 012162, <https://doi.org/10.1088/1742-6596/524/1/012162>, 2014.

830 Overland, J. E.: Prediction of Vessel Icing for Near-Freezing Sea Temperatures, *Weather and Forecasting*, 5, 62–77,
831 [https://doi.org/10.1175/1520-0434\(1990\)005<0062:POVIFN>2.0.CO;2](https://doi.org/10.1175/1520-0434(1990)005<0062:POVIFN>2.0.CO;2), 1990.

832 Overland, J. E., Pease, C. H., Preisendorfer, R. W., and Comiskey, A. L.: Prediction of Vessel Icing, *Journal of*
833 *Applied Meteorology and Climatology*, 25, 1793–1806, [https://doi.org/10.1175/1520-](https://doi.org/10.1175/1520-0450(1986)025<1793:POVI>2.0.CO;2)
834 [0450\(1986\)025<1793:POVI>2.0.CO;2](https://doi.org/10.1175/1520-0450(1986)025<1793:POVI>2.0.CO;2), 1986.

835 Parent, O. and Ilinca, A.: Anti-icing and de-icing techniques for wind turbines: Critical review, *Cold Regions*
836 *Science and Technology*, 65, 88–96, <https://doi.org/10.1016/j.coldregions.2010.01.005>, 2011.

837 Platis, A., Siedersleben, S. K., Bange, J., Lampert, A., Bärfuss, K., Hankers, R., Cañadillas, B., Foreman, R.,
838 Schulz-Stellenfleth, J., Djath, B., Neumann, T., and Emeis, S.: First in situ evidence of wakes in the far field behind
839 offshore wind farms, *Sci Rep*, 8, 2163, <https://doi.org/10.1038/s41598-018-20389-y>, 2018.

840 Powers, J. G., Klemp, J. B., Skamarock, W. C., Davis, C. A., Dudhia, J., Gill, D. O., Coen, J. L., Gochis, D. J.,
841 Ahmadov, R., Peckham, S. E., Grell, G. A., Michalakes, J., Trahan, S., Benjamin, S. G., Alexander, C. R., Dimego,
842 G. J., Wang, W., Schwartz, C. S., Romine, G. S., Liu, Z., Snyder, C., Chen, F., Barlage, M. J., Yu, W., and Duda,
843 M. G.: The Weather Research and Forecasting Model: Overview, System Efforts, and Future Directions, *Bulletin of*
844 *the American Meteorological Society*, 98, 1717–1737, <https://doi.org/10.1175/BAMS-D-15-00308.1>, 2017.

845 Pronk, V., Bodini, N., Optis, M., Lundquist, J. K., Moriarty, P., Draxl, C., Purkayastha, A., and Young, E.: Can
846 reanalysis products outperform mesoscale numerical weather prediction models in modeling the wind resource in
847 simple terrain?, *Wind Energy Sci.*, 7, 487–504, <https://doi.org/10.5194/wes-7-487-2022>, 2022.

848 Quint, D., Lundquist, J. K., Bodini, N., and Rosencrans, D.: Meteorological Impacts of Offshore Wind Turbines as
849 Simulated in the Weather Research and Forecasting Model, *Wind Energy Science Discussions*, 1–34,
850 <https://doi.org/10.5194/wes-2024-53>, 2024.

851 Rajewski, D. A., Takle, E. S., Lundquist, J. K., Oncley, S., Prueger, J. H., Horst, T. W., Rhodes, M. E., Pfeiffer, R.,
852 Hatfield, J. L., Spoth, K. K., and Doorenbos, R. K.: Crop Wind Energy Experiment (CWEX): Observations of
853 Surface-Layer, Boundary Layer, and Mesoscale Interactions with a Wind Farm, *Bulletin of the American*
854 *Meteorological Society*, 94, 655–672, <https://doi.org/10.1175/BAMS-D-11-00240.1>, 2013.

855 Redfern, S., Optis, M., Xia, G., and Draxl, C.: Offshore wind energy forecasting sensitivity to sea surface
856 temperature input in the Mid-Atlantic, *Wind Energy Science*, 8, 1–23, <https://doi.org/10.5194/wes-8-1-2023>, 2023.

857 Rosencrans, D., Lundquist, J. K., Optis, M., Rybchuk, A., Bodini, N., and Rossol, M.: Seasonal variability of wake
858 impacts on US mid-Atlantic offshore wind plant power production, *Wind Energy Science*, 9, 555–583,
859 <https://doi.org/10.5194/wes-9-555-2024>, 2024.

860 Ross, D. B. and Cardone, V.: Observations of oceanic whitecaps and their relation to remote measurements of
861 surface wind Speed, *Journal of Geophysical Research* (1896-1977), 79, 444–452,
862 <https://doi.org/10.1029/JC079i003p00444>, 1974.

863 Russell, L. M.: Sea-spray particles cause freezing in clouds, *Nature*, 525, 194–195, <https://doi.org/10.1038/525194a>,
864 2015.

865 Schneemann, J., Rott, A., Dörenkämper, M., Steinfeld, G., and Kühn, M.: Cluster wakes impact on a far-distant
866 offshore wind farm's power, *Wind Energy Science*, 5, 29–49, <https://doi.org/10.5194/wes-5-29-2020>, 2020.

867 Shcherbina, A. Y. and Gawarkiewicz, G. G.: A coastal current in winter: 2. Wind forcing and cooling of a coastal
868 current east of Cape Cod, *Journal of Geophysical Research: Oceans*, 113, <https://doi.org/10.1029/2008JC004750>,
869 2008a.

870 Shcherbina, A. Y. and Gawarkiewicz, G. G.: A coastal current in winter: Autonomous underwater vehicle
871 observations of the coastal current east of Cape Cod, *Journal of Geophysical Research: Oceans*, 113,
872 <https://doi.org/10.1029/2007JC004306>, 2008b.

873 Siedersleben, S. K., Lundquist, J. K., Platis, A., Bange, J., Bärfuss, K., Lampert, A., Cañadillas, B., Neumann, T.,
874 and Emeis, S.: Micrometeorological impacts of offshore wind farms as seen in observations and simulations,
875 *Environ. Res. Lett.*, 13, 124012, <https://doi.org/10.1088/1748-9326/aaea0b>, 2018.

876 Stull B., R.: An Introduction to Boundary Layer Meteorology, Springer Science & Business Media,
877 [https://books.google.com/books?hl=en&lr=&id=2PjrCAAQBAJ&oi=fnd&pg=PR10&dq=An+Introduction+to+Bo](https://books.google.com/books?hl=en&lr=&id=2PjrCAAQBAJ&oi=fnd&pg=PR10&dq=An+Introduction+to+Boundary+Layer+Meteorology+stull&ots=BdY_2W6EQ2&sig=eLi5IVaua4aeHUUWQt-NfG0IkTM#v=onepage&q=An%20Introduction%20to%20Boundary%20Layer%20Meteorology%20stull&f=false)
878 [undary+Layer+Meteorology+stull&ots=BdY_2W6EQ2&sig=eLi5IVaua4aeHUUWQt-](https://books.google.com/books?hl=en&lr=&id=2PjrCAAQBAJ&oi=fnd&pg=PR10&dq=An+Introduction+to+Boundary+Layer+Meteorology+stull&ots=BdY_2W6EQ2&sig=eLi5IVaua4aeHUUWQt-NfG0IkTM#v=onepage&q=An%20Introduction%20to%20Boundary%20Layer%20Meteorology%20stull&f=false)
879 [NfG0IkTM#v=onepage&q=An%20Introduction%20to%20Boundary%20Layer%20Meteorology%20stull&f=false,](https://books.google.com/books?hl=en&lr=&id=2PjrCAAQBAJ&oi=fnd&pg=PR10&dq=An+Introduction+to+Boundary+Layer+Meteorology+stull&ots=BdY_2W6EQ2&sig=eLi5IVaua4aeHUUWQt-NfG0IkTM#v=onepage&q=An%20Introduction%20to%20Boundary%20Layer%20Meteorology%20stull&f=false)
880 1988.

881 SWAN Team: Scientific and Technical Documentation (SWAN Cycle III version 41.31A), Delft University of
882 Technology, <https://swanmodel.sourceforge.io/download/zip/swantech.pdf>, 2020.

883 Tewari, M., Chen, F., Wang, W., Dudhia, J., LeMone, M., Mitchell, K., Ek, M., Gayno, G., Wegiel, J., and Cuenca,
884 R. H.: (PDF) Implementation and verification of the united NOAH land surface model in the WRF model,
885 *Proceedings of the 20th conference on weather analysis and forecasting/16th conference on numerical weather*
886 *prediction*, 14,
887 [https://www.researchgate.net/publication/286272692_Implementation_and_verification_of_the_united_NOAH_land](https://www.researchgate.net/publication/286272692_Implementation_and_verification_of_the_united_NOAH_land_surface_model_in_the_WRF_model)
888 [_surface_model_in_the_WRF_model](https://www.researchgate.net/publication/286272692_Implementation_and_verification_of_the_united_NOAH_land_surface_model_in_the_WRF_model), 2004.

889 Thompson, G., Field, P. R., Rasmussen, R. M., and Hall, W. D.: Explicit Forecasts of Winter Precipitation Using an
890 Improved Bulk Microphysics Scheme. Part II: Implementation of a New Snow Parameterization, *Monthly Weather*
891 *Review*, 136, 5095–5115, <https://doi.org/10.1175/2008MWR2387.1>, 2008.

892 Tolman, H., Abdolali, A., Accensi, M., Alves, J.-H., Arduin, F., Babanin, A., Barbariol, F., Benetazzo, A., Bidlot,
893 J., Booij, N., Boutin, G., Bunney, C., Campbell, T., Chalikov, D., Chawla, A., Cheng, S., Collins III, C., Filipot, J.-
894 F., Flampouris, S., and Liang, Z.: User manual and system documentation of WAVEWATCH III (R) version 6.07,
895 [https://www.researchgate.net/publication/336069899_User_manual_and_system_documentation_of_WAVEWATCH](https://www.researchgate.net/publication/336069899_User_manual_and_system_documentation_of_WAVEWATCH_H_III_R_version_607)
896 [H_III_R_version_607](https://www.researchgate.net/publication/336069899_User_manual_and_system_documentation_of_WAVEWATCH_H_III_R_version_607), 2019.

897 Tomaszewski, J. M. and Lundquist, J. K.: Simulated wind farm wake sensitivity to configuration choices in the
898 Weather Research and Forecasting model version 3.8.1, *Geoscientific Model Development*, 13, 2645–2662,
899 <https://doi.org/10.5194/gmd-13-2645-2020>, 2020.

900 U.S. Navy: U. S. Navy Cold Weather Handbook for Surface Ships, Surface Ship Survivability Office,
901 [https://media.defense.gov/2021/Feb/25/2002588484/-1/-1/0/CG%20070%20-](https://media.defense.gov/2021/Feb/25/2002588484/-1/-1/0/CG%20070%20-%20US%20NAVY%20COLD%20WEATHER%20HANDBOOK.PDF)
902 [%20US%20NAVY%20COLD%20WEATHER%20HANDBOOK.PDF](https://media.defense.gov/2021/Feb/25/2002588484/-1/-1/0/CG%20070%20-%20US%20NAVY%20COLD%20WEATHER%20HANDBOOK.PDF), 1988.

903 Vavrus, S., Walsh, J. E., Chapman, W. L., and Portis, D.: The behavior of extreme cold air outbreaks under
904 greenhouse warming, *International Journal of Climatology*, 26, 1133–1147, <https://doi.org/10.1002/joc.1301>, 2006.

905 Wallace, J. M. and Hobbs, P. V.: Atmospheric Science: An Introductory Survey, 2nd ed., Elsevier, University of
906 Washington, [ISBN:978-0-12-732951-2](https://doi.org/10.1016/B978-0-12-732951-2), 2006.

960 Mesoscale Impacts of Wind Farms as Parameterized in a Mesoscale NWP Model, *Monthly Weather Review*, 140,
961 3017–3038, <https://doi.org/10.1175/MWR-D-11-00352.1>, 2012.

962 Fitch, A. C., Lundquist, J. K., and Olson, J. B.: Mesoscale Influences of Wind Farms throughout a Diurnal Cycle,
963 *Mon. Wea. Rev.*, 141, 2173–2198, <https://doi.org/10.1175/MWR-D-12-00185.1>, 2013.

964 Gao, L. and Hong, J.: Wind turbine performance in natural icing environments: A field characterization, *Cold
965 Regions Science and Technology*, 181, 103193, <https://doi.org/10.1016/j.coldregions.2020.103193>, 2021.

966 Gao, L. and Hu, H.: Wind turbine icing characteristics and icing-induced power losses to utility-scale wind turbines,
967 *Proceedings of the National Academy of Sciences*, 118, e2111461118, <https://doi.org/10.1073/pnas.2111461118>,
968 2021.

969 Geerts, B., Giangrande, S. E., McFarquhar, G. M., Xue, L., Abel, S. J., Comstock, J. M., Crewell, S., DeMott, P. J.,
970 Ebell, K., Field, P., Hill, T. C. J., Hunzinger, A., Jensen, M. P., Johnson, K. L., Juliano, T. W., Kollias, P., Kosovic,
971 B., Lackner, C., Luke, E., Lüpfes, C., Matthews, A. A., Neggers, R., Ovchinnikov, M., Powers, H., Shupe, M. D.,
972 Spengler, T., Swanson, B. E., Tjernström, M., Theisen, A. K., Wales, N. A., Wang, Y., Wendisch, M., and Wu, P.:
973 The COMBLE Campaign: A Study of Marine Boundary Layer Clouds in Arctic Cold Air Outbreaks, *Bulletin of the
974 American Meteorological Society*, 103, E1371–E1389, <https://doi.org/10.1175/BAMS-D-21-0044.1>, 2022.

975 Golbazi, M., Areher, C. L., and Alessandrini, S.: Surface impacts of large offshore wind farms, *Environ. Res. Lett.*,
976 17, 064021, <https://doi.org/10.1088/1748-9326/ac6e49>, 2022.

977 Guest, P. and Luke, R.: The Power of Wind and Water, *Mariners Weather Log*,
978 https://www.vos.noaa.gov/MWL/dec_05/ves.shtml, 2005.

979 Hall, T. and Booth, J. F.: SynHETC: A Statistical Model for Severe Winter Storm Hazard on Eastern North
980 America, *Journal of Climate*, 30, 5329–5343, <https://doi.org/10.1175/JCLI-D-16-0711.1>, 2017.

981 Hersbach, H., Bell, B., Berrisford, P., Hirahara, S., Horányi, A., Muñoz-Sabater, J., Nicolas, J., Peubey, C., Radu,
982 R., Schepers, D., Simmons, A., Soci, C., Abdalla, S., Abellan, X., Balsamo, G., Bechtold, P., Biavati, G., Bidlot, J.,
983 Bonavita, M., De Chiara, G., Dahlgren, P., Dee, D., Diamantakis, M., Dragani, R., Flemming, J., Forbes, R.,
984 Fuentes, M., Geer, A., Haimberger, L., Healy, S., Hogan, R. J., Hólm, E., Janisková, M., Keeley, S., Laloyaux, P.,
985 Lopez, P., Lupu, C., Radnoti, G., de Rosnay, P., Rozum, I., Vamborg, F., Villaume, S., and Thépaut, J.-N.: The
986 ERA5 global reanalysis, *Quarterly Journal of the Royal Meteorological Society*, 146, 1999–2049,
987 <https://doi.org/10.1002/qj.3803>, 2020.

988 Hirsch, R. M., Slack, J. R., and Smith, R. A.: Techniques of trend analysis for monthly water quality data, *Water
989 Resources Research*, <https://doi.org/10.1029/WR018i001p00107>, 1982.

990 Hussain, M. M. and Mahmud, I.: pyMannKendall: a python package for non-parametric Mann-Kendall family of
991 trend tests., *Journal of Open Source Software*, 4, 1556, <https://doi.org/10.21105/joss.01556>, 2019.

992 Iacono, M. J., Delamere, J. S., Mlawer, E. J., Shephard, M. W., Clough, S. A., and Collins, W. D.: Radiative forcing
993 by long-lived greenhouse gases: Calculations with the AER radiative transfer models, *Journal of Geophysical
994 Research: Atmospheres*, 113, <https://doi.org/10.1029/2008JD009944>, 2008.

995 Kain, J. S.: The Kain–Fritsch Convective Parameterization: An Update, *Journal of Applied Meteorology and
996 Climatology*, 43, 170–181, [https://doi.org/10.1175/1520-0450\(2004\)043<0170:TKCPAU>2.0.CO;2](https://doi.org/10.1175/1520-0450(2004)043<0170:TKCPAU>2.0.CO;2), 2004.

997 Destination likely sank after accumulating ice in heavy freezing spray, report says:
998 <https://www.ktoo.org/2018/07/16/destination-likely-sank-after-accumulating-ice-in-heavy-freezing-spray-report-says/>,
999 last access: 12 April 2023.

1000 Kraj, A. G. and Bibeau, E. L.: Phases of icing on wind turbine blades characterized by ice accumulation, *Renewable
1001 Energy*, 35, 966–972, <https://doi.org/10.1016/j.renene.2009.09.013>, 2010.

1002 Lauridsen, M. J. and Ancell, B. C.: Nonlocal Inadvertent Weather Modification Associated with Wind Farms in the
1003 Central United States, *Advances in Meteorology*, 2018, e2469683, <https://doi.org/10.1155/2018/2469683>, 2018.

1004 Line, W. E., Grasso, L., Hillger, D., Dierking, C., Jacobs, A., and Shea, S.: Using NOAA Satellite Imagery to Detect
1005 and Track Hazardous Sea Spray in the High Latitudes, *Weather and Forecasting*, 37, 351–369,
1006 <https://doi.org/10.1175/WAF-D-21-0137.1>, 2022.

1007 NTSB announces the probable cause of the sunken Seandies Rose:
1008 <https://www.alaskanewsresource.com/2021/06/29/ntsb-announce-probable-cause-sunken-seandies-rose/>, last access:
1009 12 April 2023.

1010 Madi, E., Pope, K., Huang, W., and Iqbal, T.: A review of integrating ice detection and mitigation for wind turbine
1011 blades, *Renewable and Sustainable Energy Reviews*, 103, 269–281, <https://doi.org/10.1016/j.rser.2018.12.019>,
1012 2019.

1013 Martini, F., Contreras Montoya, L. T., and Ilincă, A.: Review of Wind Turbine Icing Modelling Approaches,
1014 *Energies*, 14, 5207, <https://doi.org/10.3390/en14165207>, 2021.

1015 Monahan, E. C. and MacNiocaill, G.: Oceanic Whitecaps And Their Role in Air–Sea Exchange Processes, D Reidel

016 Publishing Company, 1986.

017 Monahan, E. C., Fairall, C. W., Davidson, K. L., and Boyle, P. J.: Observed inter-relations between 10m winds,
018 ocean whitecaps and marine aerosols, *Quarterly Journal of the Royal Meteorological Society*, 109, 379–392,
019 <https://doi.org/10.1002/qj.49710946010>, 1983.

020 Monin, A. S. and Obukhov, A. M.: Basic laws of turbulent mixing in the surface layer of the atmosphere, *Tr. Akad.
021 Nauk SSSR Geophys. Inst.*, 24, 30, https://gibbs.science/efd/handouts/monin-obukhov_1954.pdf, 1954.

022 Musial, W., Spitsen, P., Duffy, P., Beiter, P., Marquis, M., Hammond, R., and Shields, M.: *Offshore Wind Market
023 Report: 2022 Edition*, National Renewable Energy Laboratory, Golden, CO (United States), 2022.

024 Nakanishi, M. and Niino, H.: An Improved Mellor–Yamada Level-3 Model: Its Numerical Stability and Application
025 to a Regional Prediction of Advection Fog, *Boundary-Layer Meteorol.*, 119, 397–407,
026 <https://doi.org/10.1007/s10546-005-9030-8>, 2006.

027 Iceing believed to cause sinking of fishing boat in Barents Sea, 17 missing:
028 [https://thebarentsobserver.com/en/2020/12/icing-believed-cause-sinking-fishing-boat-barents-sea-17-missing-last
029 access-12-April-2023](https://thebarentsobserver.com/en/2020/12/icing-believed-cause-sinking-fishing-boat-barents-sea-17-missing-last-access-12-April-2023).

030 Niu, G. Y., Yang, Z. L., Mitchell, K. E., Chen, F., Ek, M. B., Barlage, M., Kumar, A., Manning, K., Niyogi, D.,
031 Rosero, E., Tewari, M., and Xia, Y.: The community Noah land surface model with multiparameterization options
032 (Noah MP): 1. Model description and evaluation with local-scale measurements, *Journal of Geophysical Research:
033 Atmospheres*, 116, <https://doi.org/10.1029/2010JD015139>, 2011.

034 Novacheck, J., Sharp, J., Schwarz, M., Donohoo Vallett, P., Tzavelis, Z., Buster, G., and Rossol, M.: The Evolving
035 Role of Extreme Weather Events in the U.S. Power System with High Levels of Variable Renewable Energy,
036 NREL/TP-6A20-78394, 1837959, MainId:32311, NREL/TP-6A20-78394, 1837959, MainId:32311,
037 <https://doi.org/10.2172/1837959>, 2021.

038 NREL: 2023 National Offshore Wind data set (NOW-23), <https://dx.doi.org/10.25984/1821404>, 2020.

039 Glossary – NOAA’s National Weather Service: <https://w1.weather.gov/glossary/index.php?word=freezing=spray>,
040 last access: 12 April 2023.

041 Nygaard, N. G.: Wakes in very large wind farms and the effect of neighbouring wind farms, *J. Phys.: Conf. Ser.*,
042 524, 012162, <https://doi.org/10.1088/1742-6596/524/1/012162>, 2014.

043 Overland, J. E.: Prediction of Vessel Icing for Near-Freezing Sea Temperatures, *Weather and Forecasting*, 5, 62–77,
044 [https://doi.org/10.1175/1520-0434\(1990\)005<0062:POVIFN>2.0.CO;2](https://doi.org/10.1175/1520-0434(1990)005<0062:POVIFN>2.0.CO;2), 1990.

045 Overland, J. E., Pease, C. H., Preisendorfer, R. W., and Comiskey, A. L.: Prediction of Vessel Icing, *Journal of
046 Applied Meteorology and Climatology*, 25, 1793–1806, [https://doi.org/10.1175/1520-
047 0450\(1986\)025<1793:POVI>2.0.CO;2](https://doi.org/10.1175/1520-0450(1986)025<1793:POVI>2.0.CO;2), 1986.

048 Parish, T. R., Burkhart, M. D., and Rodi, A. R.: Determination of the Horizontal Pressure Gradient Force Using
049 Global Positioning System on board an Instrumented Aircraft, *Journal of Atmospheric and Oceanic Technology*, 24,
050 521–528, <https://doi.org/10.1175/JTECH1986.1>, 2007.

051 Platis, A., Siedersleben, S. K., Bange, J., Lampert, A., Bärfuss, K., Hankers, R., Cañadillas, B., Foreman, R.,
052 Schulz-Stellenfleth, J., Djath, B., Neumann, T., and Emeis, S.: First in situ evidence of wakes in the far field behind
053 offshore wind farms, *Sci Rep.*, 8, 2163, <https://doi.org/10.1038/s41598-018-20389-y>, 2018.

054 Powers, J. G., Klemp, J. B., Skamarock, W. C., Davis, C. A., Dudhia, J., Gill, D. O., Coen, J. L., Goehis, D. J.,
055 Ahmadov, R., Peckham, S. E., Grell, G. A., Michalakes, J., Trahan, S., Benjamin, S. G., Alexander, C. R., Dimego,
056 G. J., Wang, W., Schwartz, C. S., Romine, G. S., Liu, Z., Snyder, C., Chen, F., Barlage, M. J., Yu, W., and Duda,
057 M. G.: The Weather Research and Forecasting Model: Overview, System Efforts, and Future Directions, *Bulletin of
058 the American Meteorological Society*, 98, 1717–1737, <https://doi.org/10.1175/BAMS-D-15-00308.1>, 2017.

059 Pronk, V., Bodini, N., Optis, M., Lundquist, J. K., Moriarty, P., Draxl, C., Purkayastha, A., and Young, E.: Can
060 reanalysis products outperform mesoscale numerical weather prediction models in modeling the wind resource in
061 simple terrain?, *Wind Energ. Sci.*, 7, 487–504, <https://doi.org/10.5194/wes-7-487-2022>, 2022.

062 Rajewski, D. A., Takle, E. S., Lundquist, J. K., Oneley, S., Prueger, J. H., Horst, T. W., Rhodes, M. E., Pfeiffer, R.,
063 Hatfield, J. L., Spoth, K. K., and Doorenbos, R. K.: Crop Wind Energy Experiment (CWEX): Observations of
064 Surface Layer, Boundary Layer, and Mesoscale Interactions with a Wind Farm, *Bulletin of the American
065 Meteorological Society*, 94, 655–672, <https://doi.org/10.1175/BAMS-D-11-00240.1>, 2013.

066 Redfern, S., Optis, M., Xia, G., and Draxl, C.: Offshore wind energy forecasting sensitivity to sea surface
067 temperature input in the Mid-Atlantic, *Wind Energy Science*, 8, 1–23, <https://doi.org/10.5194/wes-8-1-2023>, 2023.

068 Rosenerans, D., Lundquist, J. K., Optis, M., Rybehuk, A., Bodini, N., and Rossol, M.: Annual Variability of Wake
069 Impacts on Mid-Atlantic Offshore Wind Plant Deployments [preprint], *Wind Energy Science Discussions*, 1–39,
070 <https://doi.org/10.5194/wes-2023-38>, 2023.

071 Ross, D. B. and Cardone, V.: Observations of oceanic whitecaps and their relation to remote measurements of

Commented [DR5]: Add in
<https://doi.org/10.2172/1883382>

072 surface wind Speed, *Journal of Geophysical Research* (1896–1977), 79, 444–452,
073 <https://doi.org/10.1029/JC079i003p00444>, 1974.

074 Russell, L. M.: Sea spray particles cause freezing in clouds, *Nature*, 525, 194–195, <https://doi.org/10.1038/525194a>,
075 2015.

076 Schneemann, J., Rott, A., Dörenkämper, M., Steinfeld, G., and Kühn, M.: Cluster wakes impact on a far distant
077 offshore wind farm's power, *Wind Energy Science*, 5, 29–49, <https://doi.org/10.5194/wes-5-29-2020>, 2020.

078 Sheherbina, A. Y. and Gawarkiewicz, G. G.: A coastal current in winter: 2. Wind forcing and cooling of a coastal
079 current east of Cape Cod, *Journal of Geophysical Research: Oceans*, 113, <https://doi.org/10.1029/2008JC004750>,
080 2008a.

081 Sheherbina, A. Y. and Gawarkiewicz, G. G.: A coastal current in winter: Autonomous underwater vehicle
082 observations of the coastal current east of Cape Cod, *Journal of Geophysical Research: Oceans*, 113,
083 <https://doi.org/10.1029/2007JC004306>, 2008b.

084 Siedersleben, S. K., Lundquist, J. K., Platis, A., Bange, J., Bärfuss, K., Lampert, A., Cañadillas, B., Neumann, T.,
085 and Emeis, S.: Micrometeorological impacts of offshore wind farms as seen in observations and simulations,
086 *Environ. Res. Lett.*, 13, 124012, <https://doi.org/10.1088/1748-9326/aaea0b>, 2018.

087 Stoelga, M., Sanchez-Gomez, M., Poulos, G. S., and Crescenti, J.: Estimating Long-Range External Wake Losses
088 in Energy Yield and Operational Performance Assessments Using the WRF Wind Farm Parameterization, 20,
089 [https://arcvera.com/wp-content/uploads/2022/08/ArcVera-White-Paper-Estimating-Long-Range-External-Wake-](https://arcvera.com/wp-content/uploads/2022/08/ArcVera-White-Paper-Estimating-Long-Range-External-Wake-Losses-WRF-WFP-1.0.pdf)
090 [Losses-WRF-WFP-1.0.pdf](https://arcvera.com/wp-content/uploads/2022/08/ArcVera-White-Paper-Estimating-Long-Range-External-Wake-Losses-WRF-WFP-1.0.pdf), 2022.

091 SWAN Team: Scientific and Technical Documentation (SWAN Cycle III version 41.31A), Delft University of
092 Technology, <https://swanmodel.sourceforge.io/download/zip/swantech.pdf>, 2020.

093 Tewari, M., Chen, F., Wang, W., Dudhia, J., LeMone, M., Mitchell, K., Ek, M., Gayno, G., Wegiel, J., and Cuenca,
094 R. H.: (PDF) Implementation and verification of the united NOAA land surface model in the WRF model,
095 *Proceedings of the 20th conference on weather analysis and forecasting/16th conference on numerical weather*
096 *prediction*, 14,
097 [https://www.researchgate.net/publication/286272692-Implementation-and-verification-of-the-united-NOAA-land](https://www.researchgate.net/publication/286272692-Implementation-and-verification-of-the-united-NOAA-land-surface-model-in-the-WRF-model)
098 [_surface-model-in-the-WRF-model](https://www.researchgate.net/publication/286272692-Implementation-and-verification-of-the-united-NOAA-land-surface-model-in-the-WRF-model), 2004.

099 Thompson, G., Field, P. R., Rasmussen, R. M., and Hall, W. D.: Explicit Forecasts of Winter Precipitation Using an
100 Improved Bulk Microphysics Scheme. Part II: Implementation of a New Snow Parameterization, *Monthly Weather*
101 *Review*, 136, 5095–5115, <https://doi.org/10.1175/2008MWR2387.1>, 2008.

102 Tolman, H., Abdolali, A., Accensi, M., Alves, J. H., Arduin, F., Babanin, A., Barbariol, F., Benetazzo, A., Bidlot,
103 J., Booij, N., Boutin, G., Bunney, C., Campbell, T., Chalikov, D., Chawla, A., Cheng, S., Collins III, C., Filipot, J.-
104 F., Flampouris, S., and Liang, Z.: User manual and system documentation of WAVEWATCH III (R) version 6.07,
105 [https://www.researchgate.net/publication/336069899-User-manual-and-system-documentation-of-WAVEWATCH](https://www.researchgate.net/publication/336069899-User-manual-and-system-documentation-of-WAVEWATCH-III-R-version-607)
106 [H-III-R-version-607](https://www.researchgate.net/publication/336069899-User-manual-and-system-documentation-of-WAVEWATCH-III-R-version-607), 2019.

107 Tomaszewski, J. M. and Lundquist, J. K.: Simulated wind farm wake sensitivity to configuration choices in the
108 *Weather Research and Forecasting model version 3.8.1*, *Geoscientific Model Development*, 13, 2645–2662,
109 <https://doi.org/10.5194/gmd-13-2645-2020>, 2020.

110 U.S. Navy: U. S. Navy Cold Weather Handbook for Surface Ships, Surface Ship Survivability Office, 1988.

111 Vavrus, S., Walsh, J. E., Chapman, W. L., and Portis, D.: The behavior of extreme cold air outbreaks under
112 greenhouse warming, *International Journal of Climatology*, 26, 1133–1147, <https://doi.org/10.1002/joc.1301>, 2006.

113 Wei, K., Yang, Y., Zuo, H., and Zhong, D.: A review on ice detection technology and ice elimination technology for
114 wind turbine, *Wind Energy*, 23, 433–457, <https://doi.org/10.1002/we.2427>, 2020.

115 Winters, A. C., Bosart, L. F., and Keyser, D.: Antecedent North Pacific Jet Regimes Conducive to the Development
116 of Continental U.S. Extreme Temperature Events during the Cool Season, *Weather and Forecasting*, 34, 393–414,
117 <https://doi.org/10.1175/WAF-D-18-0168.1>, 2019.

118 Xia, G., Zhou, L., Freedman, J. M., Roy, S. B., Harris, R. A., and Cervarich, M. C.: A case study of effects of
119 atmospheric boundary layer turbulence, wind speed, and stability on wind farm induced temperature changes using
120 observations from a field campaign, *Clim Dyn*, 46, 2179–2196, <https://doi.org/10.1007/s00382-015-2696-9>, 2016.

121 Alexander, M. and Scott, J.: The influence of ENSO on air-sea interaction in the Atlantic, *Geophysical Research*
122 *Letters*, 29, 461–464, <https://doi.org/10.1029/2001GL014347>, 2002.

123 Archer, C. L., Colle, B. A., Veron, D. L., Veron, F., and Sienkiewicz, M. J.: On the predominance of unstable
124 atmospheric conditions in the marine boundary layer offshore of the U.S. northeastern coast, *Journal of Geophysical*
125 *Research: Atmospheres*, 121, 8869–8885, <https://doi.org/10.1002/2016JD024896>, 2016.

126 Archer, C. L., Wu, S., Ma, Y., and Jiménez, P. A.: Two Corrections for Turbulent Kinetic Energy Generated by
127 Wind Farms in the WRF Model, *Monthly Weather Review*, 148, 4823–4835, <https://doi.org/10.1175/MWR-D-20->

Formatted: Normal, No widow/orphan control, Don't adjust space between Latin and Asian text, Don't adjust space between Asian text and numbers

128 0097.1, 2020.

129 Atkinson, B. W. and Wu Zhang, J.: Mesoscale shallow convection in the atmosphere, *Reviews of Geophysics*, 34,

130 403–431, <https://doi.org/10.1029/96RG02623>, 1996.

131 Ballot, B. and Didericus, C. H.: Note sur le rapport de l'intensité et de la direction du vent avec les écarts simultanés

132 du baromètre, *Compt. Rend.*, 765–768, 1857.

133 Battisti, L., Fedrizzi, R., Brighenti, A., and Laakso, T.: Sea ice and icing risk for offshore wind turbines,

134 *Proceedings of the OWEMES*, 20–22,

135 <https://citeseerx.ist.psu.edu/document?repid=rep1&type=pdf&doi=8bb110a8c86abf785b1b019dce37150f09de90ae>,

136 2006.

137 Beiter, P., Musial, W., Duffy, P., Cooperman, A., Shields, M., Heimiller, D., and Optis, M.: The Cost of Floating

138 Offshore Wind Energy in California Between 2019 and 2032, 2020.

139 Bodini, N., Lundquist, J. K., and Kirincich, A.: U.S. East Coast Lidar Measurements Show Offshore Wind Turbines

140 Will Encounter Very Low Atmospheric Turbulence, *Geophysical Research Letters*, 46, 5582–5591,

141 <https://doi.org/10.1029/2019GL082636>, 2019.

142 Bodini, N., Optis, M., Redfern, S., Rosenerans, D., Rybchuk, A., Lundquist, J. K., Pronk, V., Castagneri, S.,

143 Purkayastha, A., Draxl, C., Krishnamurthy, R., Young, E., Roberts, B., Rosenlieb, E., and Musial, W.: The 2023

144 National Offshore Wind data set (NOW-23), *Earth System Science Data*, 16, 1965–2006,

145 <https://doi.org/10.5194/essd-16-1965-2024>, 2024.

146 Chapman, D. C., Barth, J. A., Beardley, R. C., and Fairbanks, R. G.: On the Continuity of Mean Flow between the

147 Scotian Shelf and the Middle Atlantic Bight, *Journal of Physical Oceanography*, 16, 758–772,

148 [https://doi.org/10.1175/1520-0485\(1986\)016<0758:OTCOMF>2.0.CO;2](https://doi.org/10.1175/1520-0485(1986)016<0758:OTCOMF>2.0.CO;2), 1986.

149 Cohen, J., Zhang, X., Francis, J., Jung, T., Kwok, R., Overland, J., Ballinger, T. J., Bhatt, U. S., Chen, H. W.,

150 Coumou, D., Feldstein, S., Gu, H., Handorf, D., Henderson, G., Ionita, M., Kretschmer, M., Laliberte, F., Lee, S.,

151 Linderholm, H. W., Maslowski, W., Peings, Y., Pfeiffer, K., Rigor, I., Semmler, T., Stroeve, J., Taylor, P. C.,

152 Vavrus, S., Vihma, T., Wang, S., Wendisch, M., Wu, Y., and Yoon, J.: Divergent consensus on Arctic

153 amplification influence on midlatitude severe winter weather, *Nat. Clim. Chang.*, 10, 20–29,

154 <https://doi.org/10.1038/s41558-019-0662-y>, 2020.

155 Contreras Montoya, L. T., Lain, S., and Hinea, A.: A Review on the Estimation of Power Loss Due to Icing in Wind

156 Turbines, *Energies*, 15, 1083, <https://doi.org/10.3390/en15031083>, 2022.

157 Dehghani-Sanij, A. R., Dehghani, S. R., Naterer, G. F., and Muzychka, Y. S.: Sea spray icing phenomena on marine

158 vessels and offshore structures: Review and formulation, *Ocean Engineering*, 132, 25–39,

159 <https://doi.org/10.1016/j.oceaneng.2017.01.016>, 2017.

160 Donlon, C. J., Martin, M., Stark, J., Roberts-Jones, J., Fiedler, E., and Wimmer, W.: The Operational Sea Surface

161 Temperature and Sea-Ice Analysis (OSTIA) system, *Remote Sensing of Environment*, 116, 140–158,

162 <https://doi.org/10.1016/j.rse.2010.10.017>, 2012.

163 Ferrel, W.: *Nashville Journal of Medicine and Surgery*, 11, 7–19,

164 <https://emplocal.ex.ac.uk/people/staff/gv219/classics.d/ferrel-nashville56.pdf>, 1856.

165 Ferrier, B. S., Jin, Y., Lin, Y., Black, T., Rogers, E., and DiMego, G.: Implementation of a new grid-scale cloud and

166 precipitation scheme in the NCEP Eta model, *Amer. Meteor. Soc. Conf. on Weather Analysis and Forecasting*, 19,

167 https://scholar.google.com/scholar?hl=en&as_sdt=0%2C6&q=Implementation+of+a+new+grid-scale+cloud+and+precipitation+scheme+in+the+NCEP+Eta+model&btnG=, 2002.

168 Fitch, A. C., Olson, J. B., Lundquist, J. K., Dudhia, J., Gupta, A. K., Michalakes, J., and Barstad, I.: Local and

169 Mesoscale Impacts of Wind Farms as Parameterized in a Mesoscale NWP Model, *Monthly Weather Review*, 140,

170 3017–3038, <https://doi.org/10.1175/MWR-D-11-00352.1>, 2012.

171 Fitch, A. C., Lundquist, J. K., and Olson, J. B.: Mesoscale Influences of Wind Farms throughout a Diurnal Cycle,

172 *Mon. Wea. Rev.*, 141, 2173–2198, <https://doi.org/10.1175/MWR-D-12-00185.1>, 2013.

173 Gao, L. and Hong, J.: Wind turbine performance in natural icing environments: A field characterization, *Cold*

174 *Regions Science and Technology*, 181, 103193, <https://doi.org/10.1016/j.coldregions.2020.103193>, 2021.

175 Gao, L. and Hu, H.: Wind turbine icing characteristics and icing induced power losses to utility-scale wind turbines,

176 *Proceedings of the National Academy of Sciences*, 118, e2111461118, <https://doi.org/10.1073/pnas.2111461118>,

177 2021.

178 Geerts, B., Giangrande, S. E., McFarquhar, G. M., Xue, L., Abel, S. J., Comstock, J. M., Crewell, S., DeMott, P. J.,

179 Ebell, K., Field, P., Hill, T. C. J., Hunzinger, A., Jensen, M. P., Johnson, K. L., Juliano, T. W., Kollias, P., Kosovic,

180 B., Lackner, C., Luke, E., Lüpkes, C., Matthews, A. A., Neggers, R., Ovchinnikov, M., Powers, H., Shupe, M. D.,

181 Spengler, T., Swanson, B. E., Tjernström, M., Theisen, A. K., Wales, N. A., Wang, Y., Wendisch, M., and Wu, P.:

182 The COMBLE Campaign: A Study of Marine Boundary Layer Clouds in Arctic Cold Air Outbreaks, *Bulletin of the*

184 American Meteorological Society, 103, E1371–E1389, <https://doi.org/10.1175/BAMS-D-21-0044.1>, 2022.

185 Golbazi, M., Areher, C. L., and Alessandrini, S.: Surface impacts of large offshore wind farms, *Environ. Res. Lett.*,
186 17, 064021, <https://doi.org/10.1088/1748-9326/ac6e49>, 2022.

187 Gómez, B. and Miguez Macho, G.: The impact of wave number selection and spin-up time in spectral nudging,
188 *Quarterly Journal of the Royal Meteorological Society*, 143, 1772–1786, <https://doi.org/10.1002/qj.3032>, 2017.

189 Guest, P. and Luke, R.: The Power of Wind and Water, *Mariners Weather Log*,
190 https://www.vos.noaa.gov/MWL/dec_05/ves.shtml, 2005.

191 Hall, T. and Booth, J. F.: SynthETC: A Statistical Model for Severe Winter Storm Hazard on Eastern North
192 America, *Journal of Climate*, 30, 5329–5343, <https://doi.org/10.1175/JCLI-D-16-0711.1>, 2017.

193 Hersbach, H., Bell, B., Berrisford, P., Hirahara, S., Horányi, A., Muñoz-Sabater, J., Nicolas, J., Peubey, C., Radu,
194 R., Schepers, D., Simmons, A., Soci, C., Abdalla, S., Abellan, X., Balsamo, G., Bechtold, P., Biavati, G., Bidlot, J.,
195 Bonavita, M., De Chiara, G., Dahlgren, P., Dee, D., Diamantakis, M., Dragani, R., Flemming, J., Forbes, R.,
196 Fuentes, M., Geer, A., Haimberger, L., Healy, S., Hogan, R. J., Hólm, E., Janisková, M., Keeley, S., Laloyaux, P.,
197 Lopez, P., Lupu, C., Radnoti, G., de Rosnay, P., Rozum, I., Vamborg, F., Villaume, S., and Thépaut, J.-N.: The
198 ERA5 global reanalysis, *Quarterly Journal of the Royal Meteorological Society*, 146, 1999–2049,
199 <https://doi.org/10.1002/qj.3803>, 2020.

200 Hirsch, R. M., Slack, J. R., and Smith, R. A.: Techniques of trend analysis for monthly water quality data, *Water*
201 *Resources Research*, <https://doi.org/10.1029/WR018i001p00107>, 1982.

202 Hussain, M. M. and Mahmud, I.: pyMannKendall: a python package for non-parametric Mann-Kendall family of
203 trend tests., *Journal of Open-Source Software*, 4, 1556, <https://doi.org/10.21105/joss.01556>, 2019.

204 Iacono, M. J., Delamere, J. S., Mlawer, E. J., Shephard, M. W., Clough, S. A., and Collins, W. D.: Radiative forcing
205 by long-lived greenhouse gases: Calculations with the AER radiative transfer models, *Journal of Geophysical*
206 *Research: Atmospheres*, 113, <https://doi.org/10.1029/2008JD009944>, 2008.

207 ISO: Atmospheric Icing of Structures, Geneva, Switzerland, 2017.

208 Kain, J. S.: The Kain–Fritsch Convective Parameterization: An Update, *Journal of Applied Meteorology and*
209 *Climatology*, 43, 170–181, [https://doi.org/10.1175/1520-0450\(2004\)043<0170:TKCPAU>2.0.CO;2](https://doi.org/10.1175/1520-0450(2004)043<0170:TKCPAU>2.0.CO;2), 2004.

210 Destination likely sank after accumulating ice in heavy freezing spray, report says:
211 [https://www.ktoo.org/2018/07/16/destination-likely-sank-after-accumulating-ice-in-heavy-freezing-spray-report-](https://www.ktoo.org/2018/07/16/destination-likely-sank-after-accumulating-ice-in-heavy-freezing-spray-report-says/)
212 [says/, last access: 12 April 2023](https://www.ktoo.org/2018/07/16/destination-likely-sank-after-accumulating-ice-in-heavy-freezing-spray-report-says/).

213 Kraj, A. G. and Bibeau, E. L.: Phases of icing on wind turbine blades characterized by ice accumulation, *Renewable*
214 *Energy*, 35, 966–972, <https://doi.org/10.1016/j.renene.2009.09.013>, 2010.

215 Line, W. E., Grasso, L., Hillger, D., Dierking, C., Jacobs, A., and Shea, S.: Using NOAA Satellite Imagery to Detect
216 and Track Hazardous Sea Spray in the High Latitudes, *Weather and Forecasting*, 37, 351–369,
217 <https://doi.org/10.1175/WAF-D-21-0137.1>, 2022.

218 NTSB announces the probable cause of the sunken Seandies Rose:
219 <https://www.alaskasnewsresource.com/2021/06/29/ntsb-announce-probable-cause-sunken-seandies-rose/>, last access:
220 12 April 2023.

221 Madi, E., Pope, K., Huang, W., and Iqbal, T.: A review of integrating ice detection and mitigation for wind turbine
222 blades, *Renewable and Sustainable Energy Reviews*, 103, 269–281, <https://doi.org/10.1016/j.rser.2018.12.019>,
223 2019.

224 Martini, F., Contreras Montoya, L. T., and Ilincă, A.: Review of Wind Turbine Icing Modelling Approaches,
225 *Energies*, 14, 5207, <https://doi.org/10.3390/en14165207>, 2021.

226 Monahan, E. C. and MacNiocaill, G.: Oceanic Whitecaps And Their Role in Air-Sea Exchange Processes, D Reidel
227 Publishing Company, 1986.

228 Monahan, E. C., Fairall, C. W., Davidson, K. L., and Boyle, P. J.: Observed inter-relations between 10m winds,
229 ocean whitecaps and marine aerosols, *Quarterly Journal of the Royal Meteorological Society*, 109, 379–392,
230 <https://doi.org/10.1002/qj.49710946010>, 1983.

231 Monin, A. S. and Obukhov, A. M.: Basic laws of turbulent mixing in the surface layer of the atmosphere, *Tr. Akad.*
232 *Nauk SSSR Geophys. Inst.*, 24, 30, https://gibbs.science/efd/handouts/monin-obukhov_1954.pdf, 1954.

233 Musial, W., Spitsen, P., Duffy, P., Beiter, P., Marquis, M., Hammond, R., and Shields, M.: Offshore Wind Market
234 Report: 2022 Edition, National Renewable Energy Laboratory, Golden, CO (United States), 2022.

235 Nakanishi, M. and Niino, H.: An Improved Mellor–Yamada Level-3 Model: Its Numerical Stability and Application
236 to a Regional Prediction of Advection Fog, *Boundary Layer Meteorol.*, 119, 397–407,
237 <https://doi.org/10.1007/s10546-005-9030-8>, 2006.

238 Icing believed to cause sinking of fishing boat in Barents Sea, 17 missing:
239 <https://thebarentsobserver.com/en/2020/12/icing-believed-cause-sinking-fishing-boat-barents-sea-17-missing/>, last

240 access: 12 April 2023.

241 Niu, G. Y., Yang, Z. L., Mitchell, K. E., Chen, F., Ek, M. B., Barlage, M., Kumar, A., Manning, K., Niyogi, D.,
 242 Rosero, E., Tewari, M., and Xia, Y.: The community Noah land surface model with multiparameterization options
 243 (Noah MP): 1. Model description and evaluation with local scale measurements, *Journal of Geophysical Research-
 244 Atmospheres*, 116, <https://doi.org/10.1029/2010JD015139>, 2011.

245 Novacheck, J., Sharp, J., Schwarz, M., Donohoo Vallett, P., Tzavelis, Z., Buster, G., and Rossol, M.: The Evolving
 246 Role of Extreme Weather Events in the U.S. Power System with High Levels of Variable Renewable Energy,
 247 NREL/TP-6A20-78394, 1837959, MainId:32311, NREL/TP-6A20-78394, 1837959, MainId:32311,
 248 <https://doi.org/10.2172/1837959>, 2021.

249 NREL: 2023 National Offshore Wind data set (NOW-23), <https://dx.doi.org/10.25984/1821404>, 2020.

250 Glossary – NOAA’s National Weather Service: <https://w1.weather.gov/glossary/index.php?word=freezing+spray>,
 251 last access: 12 April 2023.

252 Nygaard, N. G.: Wakes in very large wind farms and the effect of neighbouring wind farms, *J. Phys.: Conf. Ser.*,
 253 524, 012162, <https://doi.org/10.1088/1742-6596/524/1/012162>, 2014.

254 Overland, J. E.: Prediction of Vessel Icing for Near-Freezing Sea Temperatures, *Weather and Forecasting*, 5, 62–77,
 255 [https://doi.org/10.1175/1520-0434\(1990\)005<0062:POVIN>2.0.CO;2](https://doi.org/10.1175/1520-0434(1990)005<0062:POVIN>2.0.CO;2), 1990.

256 Overland, J. E., Pease, C. H., Preisendorfer, R. W., and Comiskey, A. L.: Prediction of Vessel Icing, *Journal of
 257 Applied Meteorology and Climatology*, 25, 1793–1806, [https://doi.org/10.1175/1520-
 258 0450\(1986\)025<1793:POVI>2.0.CO;2](https://doi.org/10.1175/1520-0450(1986)025<1793:POVI>2.0.CO;2), 1986.

259 Parent, O. and Hlinea, A.: Anti-icing and de-icing techniques for wind turbines: Critical review, *Cold Regions
 260 Science and Technology*, 65, 88–96, <https://doi.org/10.1016/j.coldregions.2010.01.005>, 2011.

261 Platis, A., Siedersleben, S. K., Bange, J., Lampert, A., Bärfuss, K., Hankers, R., Cañadillas, B., Foreman, R.,
 262 Schulz-Stellenfleh, J., Djath, B., Neumann, T., and Emeis, S.: First in situ evidence of wakes in the far field behind
 263 offshore wind farms, *Sci Rep*, 8, 2163, <https://doi.org/10.1038/s41598-018-20389-y>, 2018.

264 Powers, J. G., Klemp, J. B., Skamarock, W. C., Davis, C. A., Dudhia, J., Gill, D. O., Coen, J. L., Gochis, D. J.,
 265 Ahmadov, R., Peckham, S. E., Grell, G. A., Michalakes, J., Trahan, S., Benjamin, S. G., Alexander, C. R., Dimego,
 266 G. J., Wang, W., Schwartz, C. S., Romine, G. S., Liu, Z., Snyder, C., Chen, F., Barlage, M. J., Yu, W., and Duda,
 267 M. G.: The Weather Research and Forecasting Model: Overview, System Efforts, and Future Directions, *Bulletin of
 268 the American Meteorological Society*, 98, 1717–1737, <https://doi.org/10.1175/BAMS-D-15-00308.1>, 2017.

269 Pronk, V., Bodini, N., Optis, M., Lundquist, J. K., Moriarty, P., Draxl, C., Purkayastha, A., and Young, E.: Can
 270 reanalysis products outperform mesoscale numerical weather prediction models in modeling the wind resource in
 271 simple terrain?, *Wind Energ. Sci.*, 7, 487–504, <https://doi.org/10.5194/wes-7-487-2022>, 2022.

272 Rajewski, D. A., Takle, E. S., Lundquist, J. K., Oneley, S., Prueger, J. H., Horst, T. W., Rhodes, M. E., Pfeiffer, R.,
 273 Hatfield, J. L., Spoth, K. K., and Doorenbos, R. K.: Crop Wind Energy Experiment (CWEX): Observations of
 274 Surface Layer, Boundary Layer, and Mesoscale Interactions with a Wind Farm, *Bulletin of the American
 275 Meteorological Society*, 94, 655–672, <https://doi.org/10.1175/BAMS-D-11-00240.1>, 2013.

276 Redfern, S., Optis, M., Xia, G., and Draxl, C.: Offshore wind energy forecasting sensitivity to sea surface
 277 temperature input in the Mid Atlantic, *Wind Energy Science*, 8, 1–23, <https://doi.org/10.5194/wes-8-1-2023>, 2023.

278 Rosenerans, D., Lundquist, J. K., Optis, M., Rybehuk, A., Bodini, N., and Rossol, M.: Annual Variability of Wake
 279 Impacts on Mid-Atlantic Offshore Wind Plant Deployments [preprint], *Wind Energy Science Discussions*, 1–29,
 280 <https://doi.org/10.5194/wes-2023-38>, 2023.

281 Ross, D. B. and Cardone, V.: Observations of oceanic whitecaps and their relation to remote measurements of
 282 surface wind speed, *Journal of Geophysical Research (1896-1977)*, 79, 444–452,
 283 <https://doi.org/10.1029/JC079i003p00444>, 1974.

284 Russell, L. M.: Sea-spray particles cause freezing in clouds, *Nature*, 525, 194–195, <https://doi.org/10.1038/525194a>,
 285 2015.

286 Schneemann, J., Rott, A., Dörenkämper, M., Steinfeld, G., and Kühn, M.: Cluster wakes impact on a far-distant
 287 offshore wind farm’s power, *Wind Energy Science*, 5, 29–49, <https://doi.org/10.5194/wes-5-29-2020>, 2020.

288 Sheherbina, A. Y. and Gawarkiewicz, G. G.: A coastal current in winter: 2. Wind forcing and cooling of a coastal
 289 current east of Cape Cod, *Journal of Geophysical Research: Oceans*, 113, <https://doi.org/10.1029/2008JC004750>,
 290 2008a.

291 Sheherbina, A. Y. and Gawarkiewicz, G. G.: A coastal current in winter: Autonomous underwater vehicle
 292 observations of the coastal current east of Cape Cod, *Journal of Geophysical Research: Oceans*, 113,
 293 <https://doi.org/10.1029/2007JC004306>, 2008b.

294 Siedersleben, S. K., Lundquist, J. K., Platis, A., Bange, J., Bärfuss, K., Lampert, A., Cañadillas, B., Neumann, T.,
 295 and Emeis, S.: Micrometeorological impacts of offshore wind farms as seen in observations and simulations,

296 Environ. Res. Lett., 13, 124012, <https://doi.org/10.1088/1748-9326/aaea0b>, 2018.

297 Stull B., R.: An Introduction to Boundary Layer Meteorology, Springer Science & Business Media, 1988.

298 SWAN Team: Scientific and Technical Documentation (SWAN Cycle III version 41.31A), Delft University of

299 Technology, <https://swanmodel.sourceforge.io/download/zip/swantech.pdf>, 2020.

300 Tewari, M., Chen, F., Wang, W., Dudhia, J., LeMone, M., Mitchell, K., Ek, M., Gayno, G., Wegiel, J., and Cuenca,

301 R. H.: (PDF) Implementation and verification of the united NOAA land surface model in the WRF model,

302 Proceedings of the 20th conference on weather analysis and forecasting/16th conference on numerical weather

303 prediction, 14,

304 [https://www.researchgate.net/publication/286272692_Implementation_and_verification_of_the_united_NOAH_land](https://www.researchgate.net/publication/286272692_Implementation_and_verification_of_the_united_NOAH_land_surface_model_in_the_WRF_model)

305 [_surface_model_in_the_WRF_model](https://www.researchgate.net/publication/286272692_Implementation_and_verification_of_the_united_NOAH_land_surface_model_in_the_WRF_model), 2004.

306 Thompson, G., Field, P. R., Rasmussen, R. M., and Hall, W. D.: Explicit Forecasts of Winter Precipitation Using an

307 Improved Bulk Microphysics Scheme. Part II: Implementation of a New Snow Parameterization, *Monthly Weather*

308 *Review*, 136, 5095–5115, <https://doi.org/10.1175/2008MWR2387.1>, 2008.

309 Tolman, H., Abdolali, A., Accensi, M., Alves, J. H., Arduin, F., Babanin, A., Barbariol, F., Benetazzo, A., Bidlot,

310 J., Booij, N., Boutin, G., Bunney, C., Campbell, T., Chalikov, D., Chawla, A., Cheng, S., Collins III, C., Filipot, J.,

311 F., Flampouris, S., and Liang, Z.: User manual and system documentation of WAVEWATCH III (R) version 6.07,

312 [https://www.researchgate.net/publication/336069899_User_manual_and_system_documentation_of_WAVEWATCH](https://www.researchgate.net/publication/336069899_User_manual_and_system_documentation_of_WAVEWATCH_III_R_version_607)

313 [_III_R_version_607](https://www.researchgate.net/publication/336069899_User_manual_and_system_documentation_of_WAVEWATCH_III_R_version_607), 2019.

314 Tomaszewski, J. M. and Lundquist, J. K.: Simulated wind farm wake sensitivity to configuration choices in the

315 Weather Research and Forecasting model version 3.8.1, *Geoscientific Model Development*, 13, 2645–2662,

316 <https://doi.org/10.5194/gmd-13-2645-2020>, 2020.

317 U.S. Navy: U. S. Navy Cold Weather Handbook for Surface Ships, Surface Ship Survivability Office, 1988.

318 Vavrus, S., Walsh, J. E., Chapman, W. L., and Portis, D.: The behavior of extreme cold air outbreaks under

319 greenhouse warming, *International Journal of Climatology*, 26, 1133–1147, <https://doi.org/10.1002/joc.1301>, 2006.

320 Wei, K., Yang, Y., Zuo, H., and Zhong, D.: A review on ice detection technology and ice elimination technology for

321 wind turbine, *Wind Energy*, 23, 433–457, <https://doi.org/10.1002/we.2427>, 2020.

322 Winters, A. C., Bosart, L. F., and Keyser, D.: Antecedent North Pacific Jet Regimes Conducive to the Development

323 of Continental U.S. Extreme Temperature Events during the Cool Season, *Weather and Forecasting*, 34, 393–414,

324 <https://doi.org/10.1175/WAF-D-18-0168.1>, 2019.

325 Xia, G., Zhou, L., Freedman, J. M., Roy, S. B., Harris, R. A., and Cervarich, M. C.: A case study of effects of

326 atmospheric boundary layer turbulence, wind speed, and stability on wind farm induced temperature changes using

327 observations from a field campaign, *Clim Dyn*, 46, 2179–2196, <https://doi.org/10.1007/s00382-015-2696-9>, 2016.

328

1329

Formatted: Indent: Left: 0", First line: 0", No widow/orphan control, Don't adjust space between Latin and Asian text, Don't adjust space between Asian text and numbers